2022

Revision Total Hip Femoral Stem Micromotion and Statistical Shape Modeling of the Knee

William Fugit
University of Denver

Revision Total Hip Femoral Stem Micromotion and Statistical Shape Modeling of the Knee

Abstract

The first purpose of this thesis was to compare the amount of micromotion seen in the femoral stem in a revision total hip arthroplasty between simple loading conditions and loading conditions derived from activities of daily living, through the use of experimental and computational methods. The amount of micromotion at the bone-implant interface was larger for activities of daily living, with ranges of 200μm more than the largest simple loading conditions. The second purpose of this thesis was to compare measurements of accuracy in a statistical shape model between individual bone and joint-level models, specifically for the knee. Using computational methods, this study suggested that individual bone models produced lower amounts of errors in accuracy measurements than joint-level models, specifically when looking at similar number of modes of variation in each model. These two studies present research in the development of the next generation of implants in total joint arthroplasties.

Document Type

Thesis

Degree Name

M.S.

Department

Mechanical Engineering

First Advisor

Chadd W. Clary

Second Advisor

Peter J. Laz

Third Advisor

Dinah Loerke

Keywords

Micromotion, Orthopaedics, Revision total hip arthroplasty, Statistical shape model, Total joint replacement, Total knee arthroplasty

Subject Categories

Biological Engineering | Biomechanics and Biotransport | Biomedical Engineering and Bioengineering | Engineering

Revision Total Hip Femoral Stem Micromotion and Statistical Shape Modeling of the Knee

_____

A Thesis

Presented to

the Faculty of the Daniel Felix Ritchie School of Engineering and Computer Science

University of Denver

_____

In Partial Fulfillment

of the Requirements for the Degree

Master of Science

_____

by

William Fugit

June 2022

Advisor: Chadd W. Clary, PhD

Author: William Fugit
Title: Revision Total Hip Femoral Stem Micromotion and Statistical Shape Modeling of the Knee
Advisor: Chadd W. Clary, PhD
Degree Date: June 2022

Abstract

The first purpose of this thesis was to compare the amount of micromotion seen in the femoral stem in a revision total hip arthroplasty between simple loading conditions and loading conditions derived from activities of daily living, through the use of experimental and computational methods. The amount of micromotion at the bone-implant interface was larger for activities of daily living, with ranges of 200μm more than the largest simple loading conditions. The second purpose of this thesis was to compare measurements of accuracy in a statistical shape model between individual bone and joint-level models, specifically for the knee. Using computational methods, this study suggested that individual bone models produced lower amounts of errors in accuracy measurements than joint-level models, specifically when looking at similar number of modes of variation in each model. These two studies present research in the development of the next generation of implants in total joint arthroplasties.

Acknowledgements

I would first like to thank my advisor, Dr. Chadd Clary, for his guidance, mentorship, and support throughout my undergraduate and graduate years at the University of Denver. I would also like to thank Dr. Peter Laz for his guidance and support over the course of my undergraduate and graduate years. Additionally, I would like to thank my other committee member Dr. Dinah Loerke.

I would also like to thank all the professors, students, and faculty that are part of the Center for Orthopaedic Biomechanics and Experimental Biomechanics Lab at the University of Denver. Specifically, I would like to thank Yashar Behnam for his assistance in experimental testing and data processing throughout my research projects in both my undergraduate and graduate years. I would also like to thank Thor Andreassen for his help with setting up the LabView and the cRIO for the data collection of my micromotion study.

Finally, I would like to thank Luke Aram and the rest of the knee team at DePuy Synthes for sponsoring my Statistical Shape Modelling work and providing segmented subjects. I would also like to thank the hip team at DePuy Synthes for sponsoring my Femoral Stem Micromotion work and providing specimens and implants. I would also like to thank Riza Bayoglu for his assistance in the development of the femur and tibia statistical shape models.

Table of Contents

List of Figures

List of Tables

Chapter One: Introduction

1.1 Introduction to Revision Total Hip Arthroplasty

Total hip arthroplasty (THA) is a common orthopaedic joint reconstruction procedure performed in the United States with yearly operations predicted to increase from 498,000 in 2020 to 1,429,000 in 2040 (Singh et al., 2019). While THA is a widely successful procedure, failure still occurs from infection, dislocation, osteolysis, or loosening resulting in revision rates of about 5-10% of patients within the first 10 years after a primary THA (Gwam et al., 2017, Glassou et al., 2015). Failure within revision surgeries and implants, however, is still a prevalent issue despite the advancements in implant design and surgical techniques, with the most common failure resulting from mechanical loosening in the femoral component. (Bozic et al., 2009, Gwam et al., 2015). Mechanical or aseptic loosening results from the component becoming dislodged from the cement-bone interface or from the bone-implant interface for cementless stems. The initial stability of the femoral stem, or reduction in micromotion at the bone-implant interface is required for long-term success (Mjöberg et al., 1994).

Many studies have looked at the initial stability of the femoral stem through the use of micromotion studies due to static loading conditions to create an axial or torsional load on the stem. Most of these studies have focused on the use of linear variable transducers or the use of metal beads through CT scanning to determine the micromotion seen (Burke et al., 1991, Gortchacow et al., 2010). There have also been a few studies

that have focused on the use of digital image correlation to track micromotion throughout the cycle of these loading conditions (Small et al., 2017, Race et al., 2009). The major pitfall in these studies has been the use of static loading conditions instead of loading conditions related to activities of daily living to induce micromotion.

The goal of this study in this thesis was to use computational and experimental methods to analyze how static loading conditions compare to activities of daily living loading conditions on the micromotion of the femoral stem relative to the bone. By performing static loading conditions and loading conditions from activities of daily living, a repeated measure study was performed to compare the micromotion from each of these loading conditions.

1.2 Introduction to Statistical Shape Models

Statistical Shape Modeling (SSM) is the process of using mathematics, statistics, and computation to analyze the shape of a bone into a representation that can be used for future understandings of bone shape and morphology. SSMs are tools that have been used in the quantification of morphological variations and consideration of patient variability (Sintini et al., 2018). SSMs are used in product design and selection. Specifically, they have been used for the position and orientation of implant components in total knee arthroplasty, total hip arthroplasty, and more (Galloway et al., 2013).

The knee joint is a common SSM that is developed and studied for shape and morphological variations and joint implant design and selection. Within knee SSMs, there are two different models developed, individual bone models for the tibia and femur, or full joint models that consist of both bones being modeled as one (Pedoia et al., 2015, Cerveri et al., 2020). These two different models have both been used to solve similar

biological hypotheses, such as shape variability, kinematic comparisons, or joint implant selection and design. However, very little work has been conducted to quantify differences in the two models in the accuracy of developing SSMs. The objective of this study in this thesis was to use computational methods to quantify the accuracy with which individual bone models develop SSMs compared to joint-level models, utilizing different measures of comparison (Audenaert et al., 2019).

1.3 Thesis Objectives

The objectives of this thesis are twofold. The first set of objectives is related to the Activities of Daily Living in Revision Total Hip Femoral Stem Micromotion study:

1. Determine maximum torque due to reaming and maximum impaction of the implant for revision of total hip femoral stems.
2. Compare simple loading conditions to the loading conditions from gait and stair descent for revision of total hip femoral stems.

The secondary set of objectives is related to the Accuracy Tradeoffs between Individual and Joint-Level Statistical Shape Models of Knee Morphology study:

1. Develop statistical shape models of the tibia, femur, and joint-level knee consisting of the femur and tibia modeled as one.
2. Assess trade-offs in accuracy between statistical shape models describing the tibia and femur as individual bones and statistical shape model of the knee joint using multiple evaluation measures.

1.4 Thesis Overview

This thesis has two distinct research areas and is split accordingly. This thesis provides previous research surrounding femoral stem micromotion, as well as previous

research surrounding the comparison of individual bone statistical shape models versus joint level statistical shape models of the knee. This thesis also includes original research related to the effect of activities of daily living on femoral stem micromotion and research related to the accuracy trade-offs of individual bone and joint level statistical shape models. Chapter 2 provides a review of literature on revision total hip femoral stem micromotion to provide the reader insight into the methodology and research questions that have been previously investigated. Chapter 3 provides a review of literature on statistical shape modeling of the knee to give the reader insight into the methodology used in the development of these models and the comparisons between individual bone studies and joint level studies. Chapter 4 provides a detailed report on an original study conducted at the University of Denver to analyze the effects of activities of daily living on revision femoral stem micromotion. Chapter 5 provides a detailed report on an original study performed at the University of Denver on the comparison of accuracy between individual bone and joint level statistical shape models of the knee. Chapter 6 provides concluding remarks regarding the main findings from each of these studies and related future work.

Chapter Two: Literature Review – Revision Total Hip Femoral Stem Micromotion

2.1 Revision Total Hip Arthroplasty Overview

Total hip arthroplasty (THA) is a common orthopedic joint reconstruction procedure performed in the United States with annual procedures predicted to increase from 498,000 in 2020 to 1,429,000 in 2040 (Singh et al., 2019). Total hip arthroplasty (THA) is a procedure where the hip joint is replaced with a prosthetic joint, in the cases of hips with osteoarthritis, to restore the function of the joint, as well as to relieve pain. THA involves the surgical removal of the acetabular cartilage and subchondral bone, which resides within the cup portion of the hip and replaces it with an acetabular cup. It also removes the head and proximal neck of the femur, or the ball portion of the joint, and replaces it with a small diameter head and femoral stem. (Siopack et al., 1995).

Despite THA being a widely used and successful procedure, component failure and revision still occur, mostly as a result of infection, dislocation, osteolysis, or loosening (Gwam et al., 2017). About 5-10% of patients within the first 10 years after a primary THA are revised or sustain complications, resulting in over 50,00 revision THA procedures annually in the United States (Glassou et al., 2015). Revision THA is similar to that of a primary THA, in which it still utilizes a femoral stem and head with an acetabular component, but usually at larger sizes to account for larger bone loss when compared to that of a primary THA (Sheth et al., 2013). The burden of failure in revision

is still a prevalent issue despite the advancements in implant design and surgical techniques (Bozic et al., 2009). The most common failure in revision THA for the femoral component was mechanical loosening (Gwam et al., 2015). Mechanical or aseptic loosening refers to the component becoming dislodged from either the cement in the bone or from the bone itself for cementless components. Initial stability, as a reduction in micromotion, of the implant-bone interface is required for cementless stem long-term success (Mjöberg et al., 1994).

2.2 Modular versus Nonmodular Revision Femoral Stems

Modular and nonmodular stems are commonly used in revision THA. However, which type of stem is considered better remains up for debate (Feng et al., 2020). A modular stem consists of two parts, a femoral neck portion that the femoral head connects to, and a stem portion that resides within the shaft of the femur (Fig. 2.1).

Figure 1.1: RECLAIM® Revision Modular Hip Stem (JnJMedicalDevices.com)

The two components are connected with a male taper end on the proximal portion of the stem and a female taper end on the distal portion of the femoral neck. Nonmodular

hip stems on the other hand are manufactured as a one-piece design. The femoral neck and stem are designed together (Fig 2.2).

Figure 2.2: CORAIL® Revision Nonmodular Hip Stem (JnJMedicalDevices.com)

The selection between modular and nonmodular femoral stems for revision THAs tend to be based upon the preferences and experiences of the surgeon (Feng et al., 2020). Many studies have looked at the comparison between modular and nonmodular femoral stems for both primary and revision THAs. A study performed out of Department of Orthopaedic Surgery at the Vejle Hospital in Denmark looked at clinical outcomes, specifically the level of pain between two groups that had the two different types of hip stems. The study found that more patients in the nonmodular group had pain at the clinical follow-up than the modular group did (Mikkelsen et al., 2017). Another study performed as a retrospective observational study reviewed the ability of the stems to

restore limb length and offset, as well as a comparison of complications between the two stems. The modular hip stem did have a greater proportion of patients that had equal limb lengths and smaller offsets but was not statistically significant compared to nonmodular femoral stems. The study also concluded that there was not a significant difference in complications between the two groups (Duwelius et al., 2013). The predominant reason for complication in this study was aseptic loosening in both femoral stem groups. Another retrospective study focused on the comparison between the two femoral stems in revision scenarios, specifically evaluating the improvement of quality of life, avoiding complications, and restoring femoral bone stock. The study showed that the early and midterm survivorship of the two groups was equivalent but concluded that the modular stem was superior to the nonmodular stem in improving patient quality of life, decreased complications, and restoration of the femur (Richards et al., 2009). This study also showed that the main cause of complications for both the stems was aseptic loosening. Another study conducted at the Department of Orthopedic Surgery at the Hospital of Xuzhou Medical University in Jiangsu, China compared the two femoral stems in a revision setting as well, to assess the clinical and radiographic outcomes. The study found that there was a significantly higher occurrence of intraoperative fracture in the modular group, but also found that there was a significant increase in subsidence in the nonmodular group than the modular group (Feng et al., 2020). This study also found the leading reason for revision to be aseptic loosening for both groups.

Most of the studies that review the difference between the two femoral stems are retrospective reviews of clinical data. Very little literature discusses in vitro comparison

between the two femoral stems specifically looking at the initial stability of the femoral stem, which can be measured through micromotion.

2.3 Previous Research Surrounding Femoral Stem Micromotion

Femoral stem micromotion in THA has been studied in numerous different ways. The most common way during early testing was using electrical transducers to measure at specific points along the interface between the implant and cement interface or between the implant and bone interface for cementless femoral stems. An early methodology used electrical displacement transducers or extensometers, that consisted of a cylindrical metal pin that was press-fit into the femoral component and a hollow outer cylinder that was attached to specific parts of the bone. Then the extensometer was attached to the two pins and the motion was measured between the inner pin and outer pin (Burke et al., 1991). Similar processes were done using linearly variable transducers (LVDT) in two other publications. The LVDT is a similar tool to that explained in the Burke et al., 1991 study, consisting of a solid cylindrical pin attached to the femoral stem with an outer hollow cylindrical pin attached to the bone, and motion was captured between the two pins (Fig. 2.3) (Baleani et al., 2000; Barr et al., 2015).

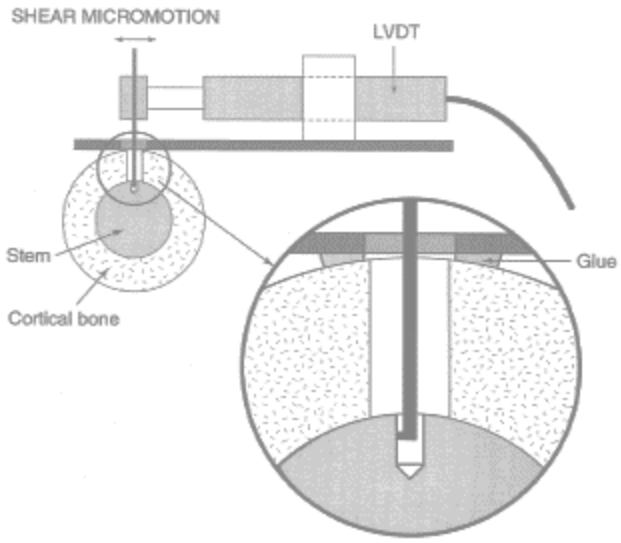

Figure 3.3: Demonstration of LVDT setup to measure micromotion at implant-bone interface (Baleani et al., 2000)

This process was a successful way of determining micromotion, however, it was reliant on the consistent placement of the LVDT for comparisons between each of the bones. It also was only able to measure micromotion at specific points along the stem and bone and not the entire implant to the bone.

Two previous studies utilized a methodology to determine the micromotion of the entire stem relative to the bone. One study, before implantation of the femoral stem, super-glued 5 tantalum beads to drilled portions of the femoral stem and attached another 15 beads through manual press-fit to the reamed-out portion of the bone-implant surface. The specimen was then placed into an aluminum fixture that enclosed the entire femur, which had a piston at the proximal end to create an axial load onto the stem (Fig 2.4). A CT scan was done before and after loading, and a registration process was performed to align the stem beads to one another to determine the displacement of the bone beads to one another (Gortchacow et al., 2010).

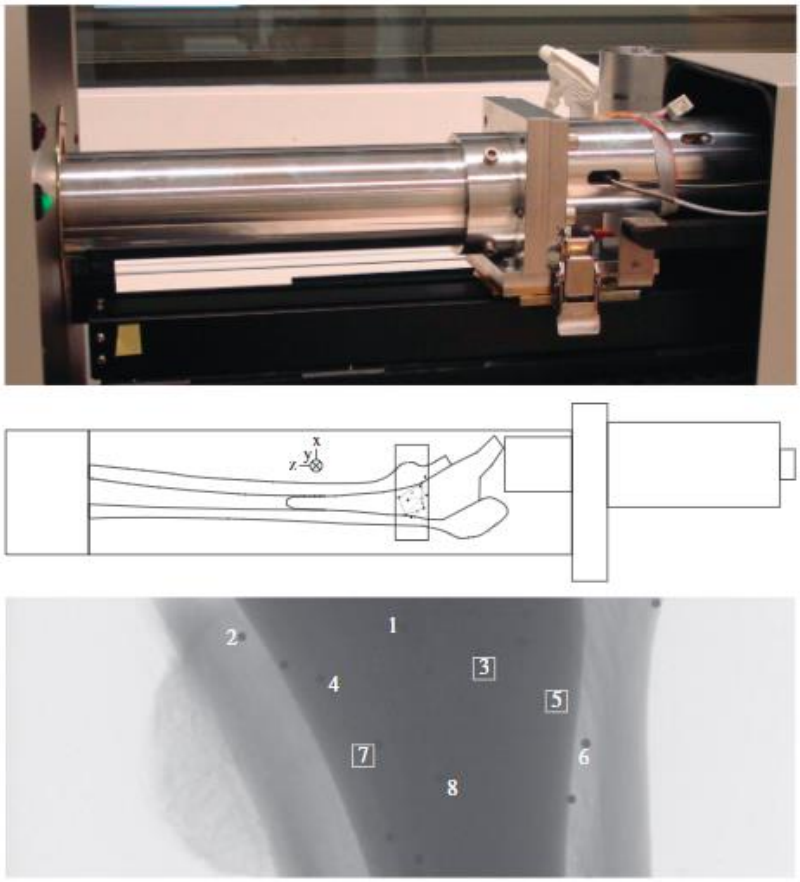

Figure 4.4: Testing setup that consisted of an aluminum enclosure with piston to develop axial loading onto the stem (Top and Middle) and a CT Scan showing placement of tantalum beads on the femoral stem and femur (Bottom) (Gortchacow et al., 2010).

Another study followed a very similar testing setup, utilizing a testing fixture close to that of Gortchacow et al., 2010 to allow for CT scanning. Similar to the previous study there were 37 tantalum beads placed on the femoral stem surface, however, this study used around 1,000 stainless steel beads manually press-fit into the metaphyseal cancellous bone. This study also had a pre- and post-CT scan for the loading of the stem, but unlike the previous study, also conducted a CT scan while the stem was being loaded. The post-processing was very similar, as well, with a rigid body registration of the implant markers and then determining displacements of the bone markers to one another

(Camine et al., 2017). Although these studies, in contrast to the LVDT studies, allow for an understanding of the micromotion of the whole stem to the femur there are still some limitations to this type of experimental design. One of the limitations comes from the metallic artifacts during scanning, which could cause issues in the registration process between CT scans, as well as, issues in displacement measurements between the markers (Gortchacow et al., 2010). Another limitation of this testing setup is the effect of the markers on the mechanical properties of the stem and bone, and also the fixation ability of the stem to the bone. Although small holes were drilled into the stem, it could still have some effect on the movement of the stem, the manually press-fit markers into the femur could cause both issues of the bone becoming weakened, as well as the decreased surface area of the stem to attach to the bone.

The use of Digital Correlation Imaging (DIC) cameras allows for studies to visualize micromotion in real-time without the need for CT scans or measurement equipment attached to the stem or bone. One study developed a testing protocol using a DIC camera system to compare micromotion in different lengths and shoulder variations for femoral stems. This study drilled 3 measurement windows, 8mm in diameter, and applied a black and white speckled pattern on the stem in these windows to track micromotion. This setup was placed into a loading apparatus to apply axial and torsional loads to the femoral head (Fig 2.4). The DIC tracking software computed point-to-point measurements to determine micromotion (Small et al., 2017).

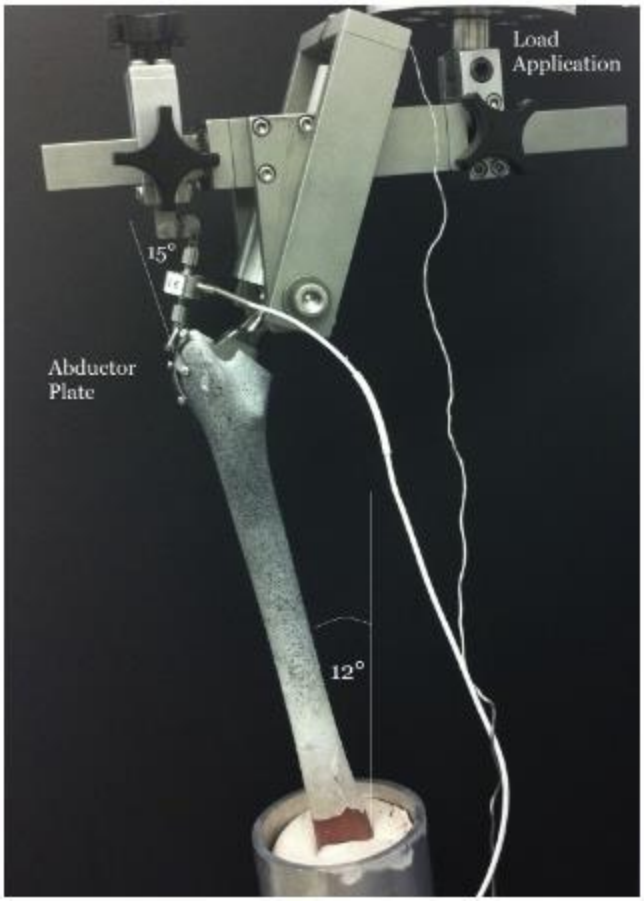

Figure 5.5: Testing setup to create axial and torsional loads at the head of the femur. Femur has white and black speckle paint for micromotion testing at specified windows (Small et al., 2017).

Another study used a very different testing setup, but still employed the use of a DIC camera for micromotion. This study, after implantation of the stem, took transverse slices at 10mm thick from the specimen, placed them into a custom torsional load device, and used a DIC system to compute micromotion at the implant-cement and cement-bone interfaces (Fig 2.5) (Race et al., 2009).

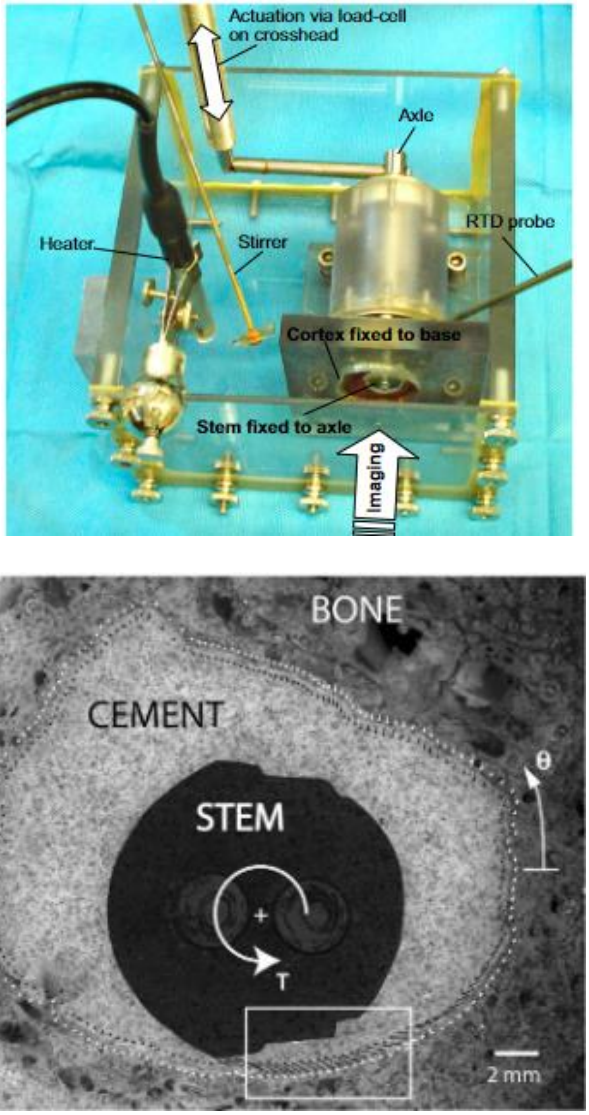

Figure 6.6: Custom torsional load setup for 10mm thick specimen slices with window for DIC camera system (Top) and an image from the DIC showing micromotion at specified interfaces (Bottom) (Race et al., 2009).

While both of these studies show the use of DIC camera systems for tracking micromotion of the stem relative to the femur without the use of equipment being placed within the specimen, they both required alterations to occur to the specimen. Small et al., 2017 required the use of viewing windows to be drilled into the bone to track micromotion, which can cause mechanical properties issues of the bone and can create

fixation issues of the stem to the bone, similar to that of both Gortchacow et al., 2010 and Camine et al., 2017 studies. Race et al., 2009 required complete geometrical change to the specimen.

Another common way micromotion is measured is through the use of finite element (FE) computation. This includes the process of segmenting CT scans to develop 3D models of the femur, aligning the femoral stem to the femur by following the surgical procedure computationally, and applying loads and boundary conditions to the stem and femur to induce micromotion (Andreaus et al., 2009; Russell et al., 2016). Although the FE methodology is consistent in predicting micromotion, it requires the need for a physical testing setup to provide validation of the models.

All of these different testing setups show different ways to both induce and measure micromotion, however the largest downfall to all of these studies is the need to alter the specimen or disturb the fixation of the stem to the bone to measure the micromotion. An accurate measurement of the micromotion between the stem and the femur as a whole will need to be done without causing any changes to the physical properties or fixation of the stem and bone. Another limitation of the previous studies is the focus on simple loading conditions, where the loading condition is only applied in one degree of freedom, such as an axial or torsional load (Gortchacow et al., 2010, Small et al., 2017). There has been very little research done around the use of loading conditions derived from activities of daily living, which may show larger amounts of micromotion comparative to simple one degree of freedom loading conditions.

Chapter Three: Literature Review – Statistical Shape Modeling of the Knee

3.1 Overview of Statistical Shape Modeling

Statistical Shape Modeling (SSM) is the process of using mathematics, statistics, and computation to parse the shape or bone into a representation that can be utilized in future testing of biologically relevant hypotheses. SSMs can be used to predict whether a specific bone can classify a group of a species, skeletal development due to gene mutation, shape changes in brain structure, the extent of bone deformation, and more (Goparaju et al., 2022). Many different clinical applications come from SSMs as well. SSMs can be used as an approach to aid in the reconstruction of shapes from measurement data such as CT or MRI (Tack et al., 2018). They are also used in the process of shape analysis, for example, to help identify specific subgroups within the population to help create treatment planning (Bruse et al., 2017). In addition, SSMs are largely used in product design and selection, for digital design, the position of the tibial component in a total knee arthroplasty, and more (Galloway et al., 2013). More specifically, SSMs are strong tools to be used in the quantification of morphological variations and consideration of patient variability (Sintini et al., 2018). SSMs, generally, are generated by registering a set of geometries to a main template of that specific bone and then applying a principal component analysis (PCA) to the registered data to develop modes of variation within the data set (Fig. 3.1) (Sintini et al., 2018).

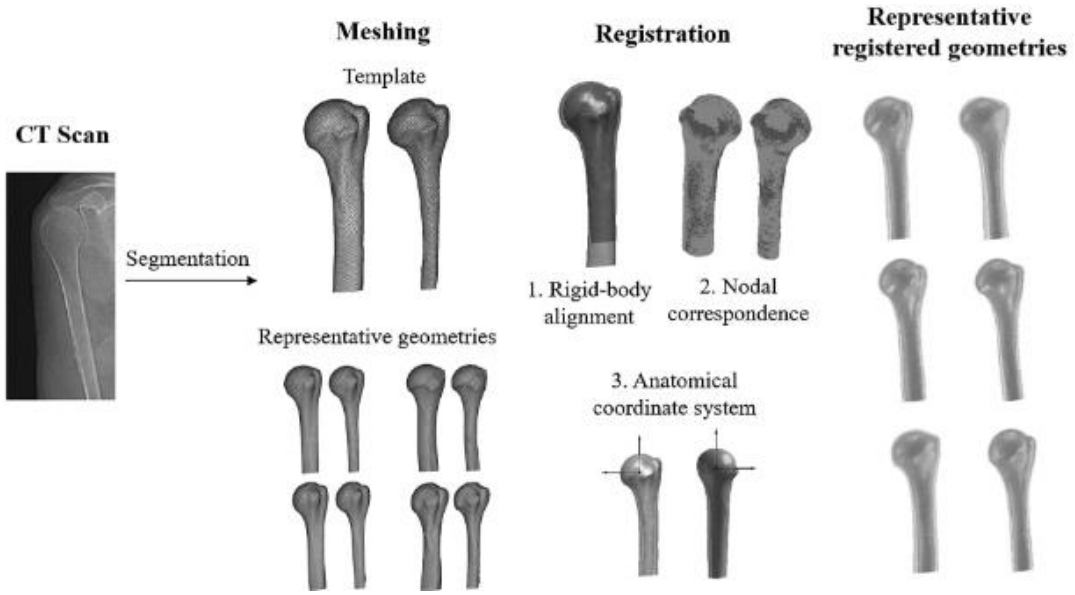

Figure 3.1 Process to register a subject set and develop an SSM (Sintini et al., 2018)

The first step is developing 3D models of the bone by segmenting the CT scans of each of the bones. Next, the registration is generally done in two parts, with the first part being a rigid-body alignment and then a second non-rigid iterative closest point. Then a PCA is applied to the registered subjects to create the SSM. This will allow for the computation of anatomical measurements across the data set (Fitzpatrick et al., 2011; Sintini et al., 2018).

3.2 Previous Literature on Individual Bone and Joint Statistical Shape Modeling

The knee joint is a common SSM that is developed and studied, and this joint will be the focus of the literature review as it pertains most to the SSM study conducted in this thesis. One of the most frequent forms of statistical shape modeling is the development of a single bone model, such as just the femur or tibia. Many previous kinds of literature have developed individual bone SSMs to study morphological variations, patient variability, and more. Within the knee joint, it is generally seen that both the femur and

tibia are developed into their respective individual SSMs and are studied separately or together. One study developed individual SSMs for the tibia and femur in order to compare relevant shapes of the tibia and femur for patients with and without anterior cruciate ligament (ACL) injuries (Fig 3.2). Within this publication, the authors analyzed the effects of ACL injuries on each of the bones individually, specifically performing a shape analysis on both the tibia and femur separately (Pedoia et al., 2015).

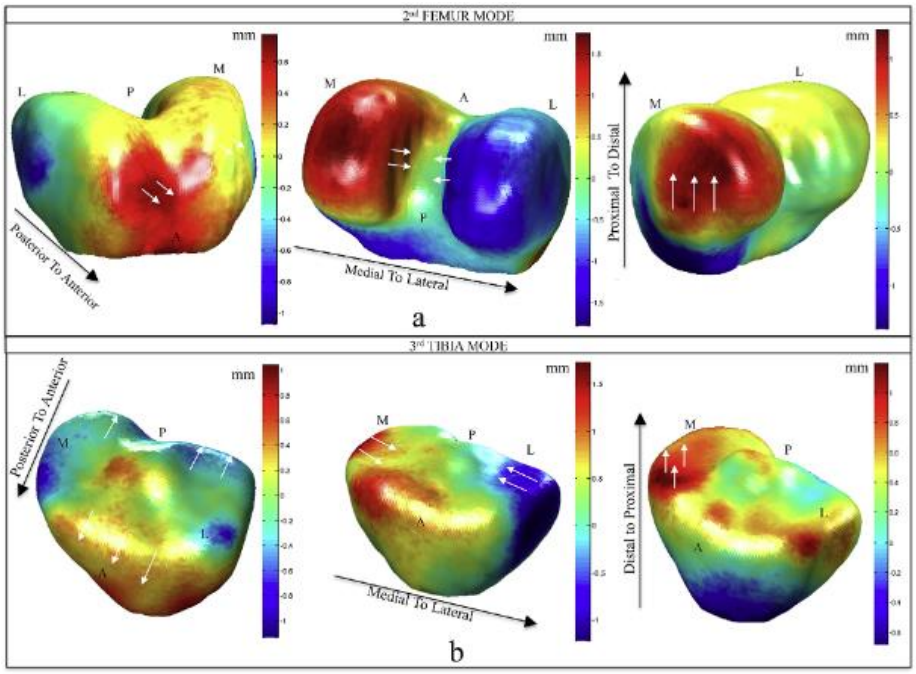

Figure 3.2 Depiction of the comparison of displacements of vertices between ACL injured subjects and healthy subjects (Pedoia et al., 2015).

Another study developed SSMs for the tibia and femur individually but reviewed the results together in order to discuss the differences in the full knee shape between women and men. Specifically, this study took into account the differences between the shape changes of the tibia and femur between the two genders and developed a scoring system to compare the changes per mode for both bones (Wise et al., 2016). Another study utilized individual SSMs for the tibia and femur to develop a new approach for

subject-specific knee shape reconstruction between multiple asynchronous fluoroscopy images from different x-ray views using a CT-based SSM. (Fig 3.4). They were directly comparing the errors between each of the fluoroscopy views to the CT-based SSM for both the tibia and femur individually and finding an overall error between the two bones for each instance of imaging (Lu et al., 2021).

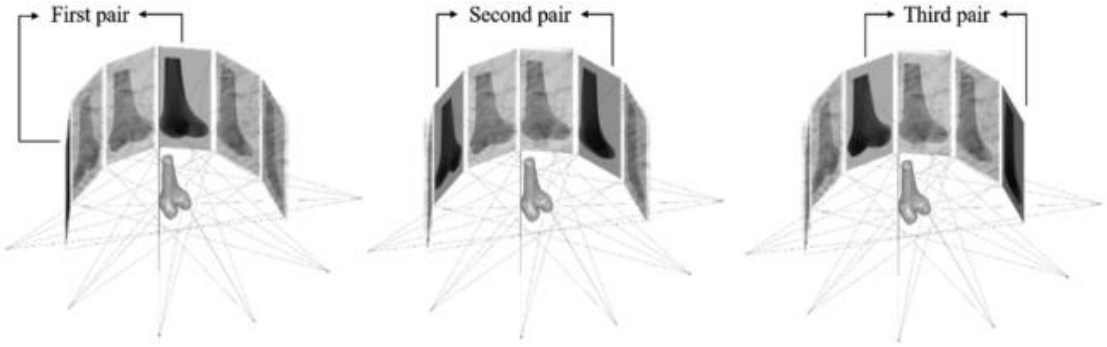

Figure 3.3 Illustration showing the different views of the fluoroscopy images that were used to develop 3D models to compare to the CT-based SSM (Lu et al., 2021).

The other form of statical shape modeling of the knee is to develop a full joint SSM. This is where the tibia and femur, and occasionally the patella or fibula depending on study objectives, are modeled as one whole geometry. One study developed a model of the knee joint that included the proximal tibia and distal femur to study and predict knee joint instability (Fig 3.5). This study was looking at the change in specific angles and slopes of the shape geometry of the SSM such as the hip-knee-ankle angle, femoral varus-valgus, tibial slope, and others to help with the prediction of instability within the knee joint (Cerveri et al., 2020).

Figure 3.4 Deviations in alignment from different modes of the knee joint SSM (Cerveri et al., 2020).

The knee is also modeled with other bones such as the patella to study the variability in alignment, as well as shape variability (Fig 3.5). Using the patella as part of the model helps with studying the changes in contact patches and anatomy of the tibial-femoral and patella-femoral articulation, and also, analyzing the kinematics within those specific contact areas (Rao et al., 2013; Smoger et al., 2015).

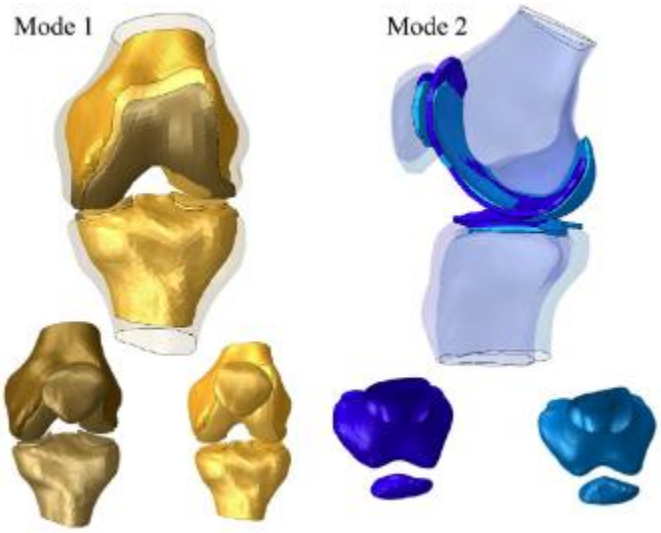

Figure 3.5 Changes in the first two modes of a full knee joint SSM with patella (Rao et al., 2013).

Full SSMs are also used to compare the kinematics of daily movement with biomechanical features of shape variation within the joint or limb, specifically through the use of a full lower limb that includes the pelvis, femur, and fibula and, depending on the study, will also include the patella. One study utilized a full lower limb SSM to quantify the relationship between features on the SSM to model-derived kinematics. This study specifically used the SSM to predict and create the geometry of the lower limb and used the model to derive kinematics for various daily living activities (Roeck et al., 2021). Another study used a lower limb SSM to develop an articulated shape model to show muscle attachment regions (Fig 3.6) (Zhang et al., 2016).

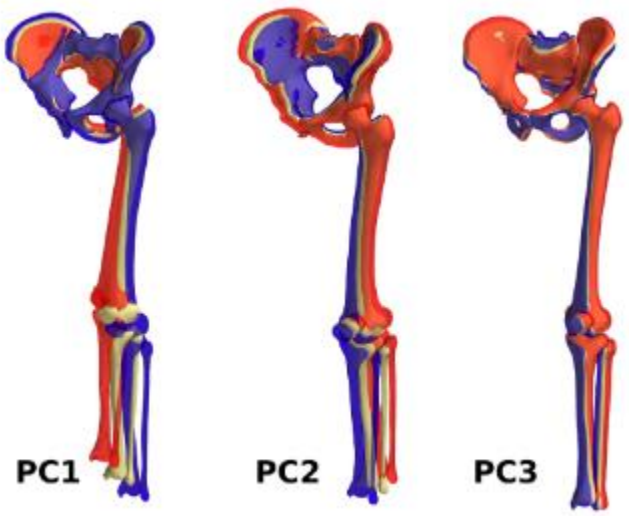

Figure 3.6 Changes in the first three modes of a full lower limb SSM (Zhang et al., 2013).

Although both types of SSMs are used for the knee joint or lower limb for similar objectives such as shape variability and kinematic comparisons, little work has been done to quantify the differences between the two models to determine which type of model is more accurate in developing SSMs. One study created an individual femur SSM and a combined tibiofemoral to compare femur cartilage reconstruction between explicit and

implicit modeling of the cartilage (Van Dijck et al., 20200). However, this study was only looking at the comparison between these two models in small areas, specifically the articulation surfaces on the tibia and femur. The study concluded that there was not a difference between the two models within the average cartilage areas. This study does provide some insight into the comparison between individual and joint SSMs, however, it is not enough evidence to determine which model is more accurate in the development of an SSM.

Chapter Four: Activities of Daily Living in Revision Total Hip Femoral Stem Micromotion

4.1 Introduction

Total hip arthroplasty (THA) is a common orthopedic joint reconstruction procedure performed in the United States with annual procedures predicted to increase from 498,000 in 2020 to 1,429,000 in 2040 (Singh et al., 2019). Despite THA being a widely used and successful procedure, component failure and revision still occur, mostly as a result of infection, dislocation, osteolysis, or loosening (Gwam et al., 2017). Cementless femoral fixation has become an increasingly more popular method used by surgeons in revision THAs. However, the most common failure in revision THA for the femoral component was mechanical loosening (Gwam et al., 2015). Initial stability of the implant-bone interface is required for cementless stem long-term success (Mjöberg 1994).

The main clinical focus behind micromotion studies is to assess the initial stability of the femoral stem after implantation. Bone-implant interface micromotions immediately after implantation are significantly related to the failure of cementless total hip arthroplasty (Gortchacow et al., 2011). This is especially important in revision THA procedures where mechanical loosening is seen in 16.8% of revision THA procedures with 22.5% of the mechanical loosening occurring at the femoral component (Gwam et al., 2017).

Femoral stem micromotion in THA has been studied in numerous different ways. The most common way during early testing was using electrical linearly variable displacement transducers (LVDT) to measure micromotion at specific points between the implant and cement interface or between the implant and bone interface for cementless femoral stems (Burke et al., 1991). This process was a successful way of determining micromotion, however, it was reliant on the consistent placement of the LVDT for comparisons between specimens. A more recent type of experimental setup consists of manually press fitting small metal beads into the femoral stem and into the femoral canal, then placing the femur and implant into a fixture setup to apply force on the stem while the fixture setup is in a CT scan to track movement of the beads to one another (Gortchacow et al., 2010). The limitation of this type of study comes from the metallic artifacts during scanning, which could cause issues in the registration process between CT scans, as well as issues in displacement measurements between the markers. Recently the most common studies consisted of the use of Digital Image Correlation (DIC) cameras which allow for studies to visualize micromotion in real-time without the need for CT scans or physical sensors attached to the stem or bone. The femur with femoral stem implanted are put into testing setups to apply load to the stem with DIC stickers or black-and-white speckle pattern applied to the stem and bone for the DIC camera system to track micromotions (Small et al., 2017). Most of these studies have altered the bone in order to track micromotions of the stem distally, such as drilling out a window to view the movement of the stem, however, this causes mechanical changes to the stability of the stem relative to the bone.

One of the largest limitations of the previous revision femoral stem micromotion studies is the focus on simple loading conditions, where cyclic loading conditions are applied to the stem in only one degree of freedom, such as an SI load. Most studies have not looked at the comparison between simple loading conditions and the loading conditions from activities of daily living. The objective of this study was to compare micromotion between simple loading conditions to dynamic gait and stair descent loading on both modular and nonmodular revision THA femoral stems. It was hypothesized that there would be larger amounts of micromotion in the gait and stair descent loading conditions when compared to the simple loading conditions.

4.2 Methods

Specimen Preparation

Six matched pairs of fresh-frozen right and left cadaveric human femurs (12 total) were tested in this experiment, with specimen demographics shown in Table 1.

Table 4.1 Specimen List Demographics

Specimen #	Specimen ID	Age	Sex	Height (in)	Weight (lbs)
1	L210430	73	F	63	122
2	L210435	65	M	70	236
3	L210443	64	M	64	100
4	S210681	61	F	67	248
5	S211705	48	F	67	216
6	S211834	59	F	65	207

The femurs were resected 175mm distally from the center of the femoral head to accommodate implantation of 140mm revision femoral stems. Using a plumb line, the femoral heads were aligned directly above the center of a cylindrical fixture and the distal femoral shaft at the bottom-center of the fixture, then cemented in place using fast-setting epoxy. A fiducial marker with a 3-mm hemispherical indention was screwed into the

greater trochanter to aid in registration. The femur assemblies were scanned with a white-light scanner (Artec Space Spider, Artec3D, Santa Clara, CA), including the native bone, fixture, fiducial maker, and a triad of hemispherical indentions on the fixture used for registration of the scan with kinematics measured during testing. All specimens underwent preoperative CT scans and 3D models for each femur were created using ScanIP (Synopsys, Mountain View, CA).

Each femur was implanted with a cementless revision femoral stem. For matched pairs of femurs, the first side was implanted with a *modular* RECLAIM® stem (DePuy Synthes, Warsaw, IN) and the contralateral side was implanted with a *non-modular* RECLAIM® stem (DePuy Synthes, Warsaw, IN). The implantation process consisted of first resecting the femoral head, then broaching for a properly-sized primary stem (ACTUS®, DePuy Synthes, Warsaw, IN) in order to create a cavity in the femur typical for revision THA. The femur was then reamed for a revision stem and the implant was impacted into the femoral cavity.

A 6 degree of freedom load cell (Kistler Instrument Corp, Novi, MI) was mounted beneath the fixtured femur to measure loading during reaming and impaction. Data from the load cell was recorded at a sampling rate of 10kHz with a custom LabView script (National Instruments, Austin, TX). Simultaneously, a motion capture system (Optotrak Certus™, NDI, Ontario, Canada) was used to track rigid arrays of infrared emitting diodes (IREDs) attached to the reaming drill and implant impactors, and the femoral bone fixture. To register the instrument geometry, specimen, and load cell to the kinematic tracking arrays, multiple circular target stickers were placed on the surfaces of the drill and impactor. Likewise, 3-mm hemispherical indentions were machined on the surfaces

of the fixturing and load cell. The instruments, fixtures, and specimen were scanned with an optical scanner to develop 3D models of the parts and to digitize the 3D coordinates of the target stickers and indentations. During testing, a digitizing probe was used to identify these same landmarks relative to their respective optical tracking arrays. A singular value decomposition (SVD) algorithm was used to align the digitized points on the solid models to those recorded during the physical experiment. The proximal femoral geometry was re-scanned after reaming to digitize the calcar resection geometry.

Micromotion Testing

In preparation for micromotion testing, ten 0.8mm diameter DIC target stickers were placed along the exposed proximal portion of the femoral stem. Another ten DIC stickers were placed on the proximal portion of the femur along the calcar resection. The specimens were then optically scanned a final time with the DIC stickers applied to record the implanted stem orientation and target sticker position (Figure 4.1).

Figure 4.1 Optical Scan of specimen with DIC stickers applied to femoral stem and femur bone.

Each implanted specimen was placed into the VIVO simulator (AMTI, Waterton, MA). Custom-developed acetabular fixturing incorporated a PINNACLE ® Acetabular Cup (Size 52mm) with an ALTRX® Liner (32mm inner diameter, DePuy Synthes, Warsaw, IN) oriented 180° to the stage of the VIVO, to allow for load application to the stem via the femoral head (Figure 4.2). Each specimen used the same DePuy Synthes Standard Metal Femoral Head (Size 32, DePuy Synthes, Warsaw, IN).

Figure 4.2 Micromotion testing fixture setup in the AMTI VIVO.

Specimen were loaded with a sequence of loading conditions applied to the femoral head via the acetabular fixture:

- Pre-conditioned with a 200N sinusoidal superior-inferior (SI) force at 0.5Hz for 200 cycles.
- Trapezoidal load in the anterior-posterior (AP) direction, with magnitudes of ±50N, ±100N, and ±150N, coupled with a constant medial load of 25N

and inferior load of 100N to ensure the head was seated in the acetabular liner (Figure 4.3).

- Trapezoidal load in the inferior direction ranging from 100N to either 400N, 900N, 1300N, or 1700N, with a constant medial load of 25N (Figure 4.3).
- Gait and Stair Descent loads from the Orthoload Database at 50% and 100% of the loads for a 75kg subject (Figure 4.4).

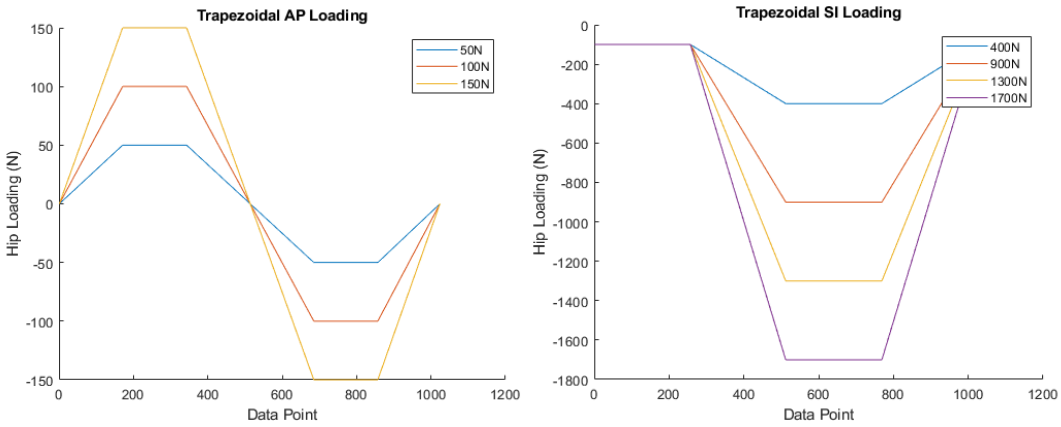

Figure 4.3 Trapezoidal loading conditions for AP (left) and SI (right).

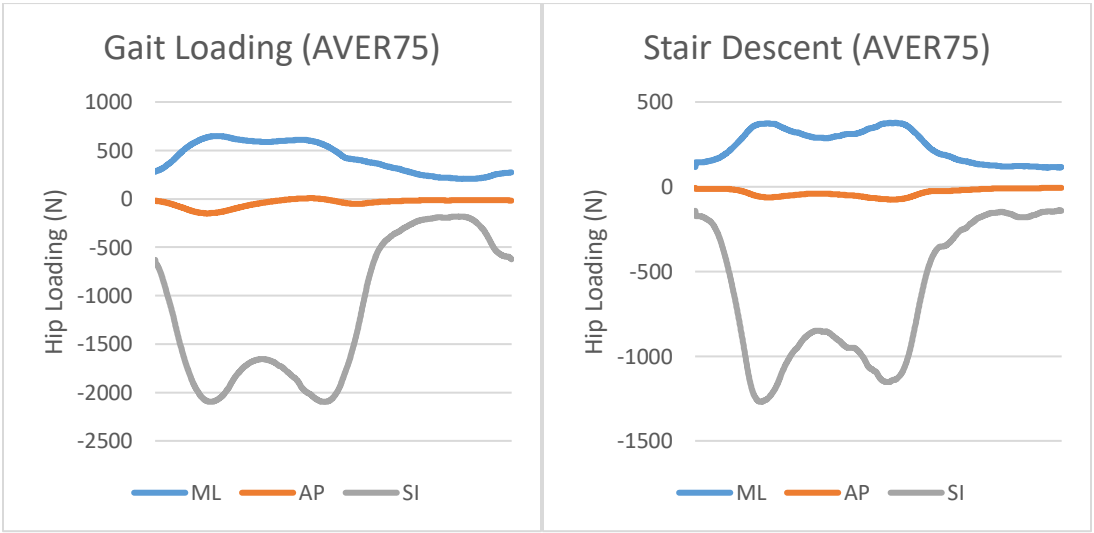

Figure 4.4 Loading conditions for Gait (left) and Stair Descent (right) at 100%.

All loading conditions were applied for 5 cycles at 0.1Hz (Figures 4.3 and 4.4). The last two cycles of each loading condition were recorded using a GOM Aramis (GOM, Braunschweig, DE) DIC camera system to track the coordinates of the target stickers on the bone implant interface at 20Hz.

Post-Processing – Implantation Loading

The segmented 3D models of the femurs from the CT scans were registered to the bony geometries from each of the optical scans. A Femoral Local Coordinate System (LCS) was created using the epicondylar axis and an axis along the proximal portion of the femoral shaft from the femoral anatomy, with the SI axis (z-axis) of the coordinate system along the femoral shaft axis and rotationally aligned with the x-axis along the epicondylar axis. The load cell LCS and the solid models of the reaming and impaction devices were transformed into the femoral LCS during each step of the surgical process using the optical tracking data from the Optotrack. The reamer torque during each reaming sequence was calculated as the dot product of the moment vector recorded by the load cell and the axis of the reamer calculated from the drill solid model. The maximum torque for the final reaming for each specimen was determined and was designated to two different groups for each implant type. A paired sample t-test was conducted to determine the p-value between the two different implants for the reaming torques.

To analyze the impaction data, a peak detection algorithm was used to identify the start and end of each mallet strike and the peak force during the strike. Femur advancement with each mallet strike was calculated by transforming the most distal point on the impaction handle (where it attaches to the implant) into the femoral LCS and calculating the change in SI position before and after each strike. The final impaction

force was determined by finding the last time a mallet strike advanced the stem into the bone and recording the force during this impaction event was designated to two different groups for each implant type. A paired sample t-test was conducted to determine the p-value between the two different implants for the impaction forces.

Post-Processing – Implant Micromotion

Computer Aided Design (CAD) models of stem geometry were oriented with the origin at the most proximal end of the stem and the stem axis aligned in the SI axis. The implanted stem geometry and femoral bony anatomy reconstructed from the optical scans captured during the experiment was then aligned to the CAD models using an iterative closest point algorithm on the common surfaces (Artec3D, Santa Clara, CA) to establish a neutral unloaded orientation between the femur bone and stem. 3D coordinates of the target stickers on the stem and bone were extracted in the implant coordinate system from the aligned optical scans.

To calculate the implant micromotion, the 3D position of the implant and bone DIC targets for each frame of each loading condition recorded by the DIC cameras were analyzed. An initial transformation was calculated to align the stem DIC targets to the stem CAD geometry in the implant coordinate system ($TM_{DIC\ to\ Implant}$) using singular value decomposition (SVD). This transformation was applied to both the stem and bone DIC target coordinates. A subsequent SVD was then performed to calculate the transformation between bone DIC targets in the neutral unloaded pose and in the loaded pose for each frame ($TM_{BoneUnloaded\text{-}to\text{-}BoneLoaded}$) (Figure 4.5). Grood & Suntay kinematics were calculated from the $TM_{BoneUnloaded\text{-}to\text{-}BoneLoaded}$ to decompose the directions of the relative micromotion between the stem and bone into an anatomic description (Grood and

Suntay, 1983). The kinematics were assembled into two groups per loading condition, one for each type of implant, and the mean and standard deviation for each kinematic per different loading condition was calculated individually for the modular and non-modular stem. Two-way analyses of variance (ANOVA) with Tukey's post-hoc tests were conducted to determine statistically significant differences in micromotion between implant types and loading conditions for the kinematics ($p<0.05$).

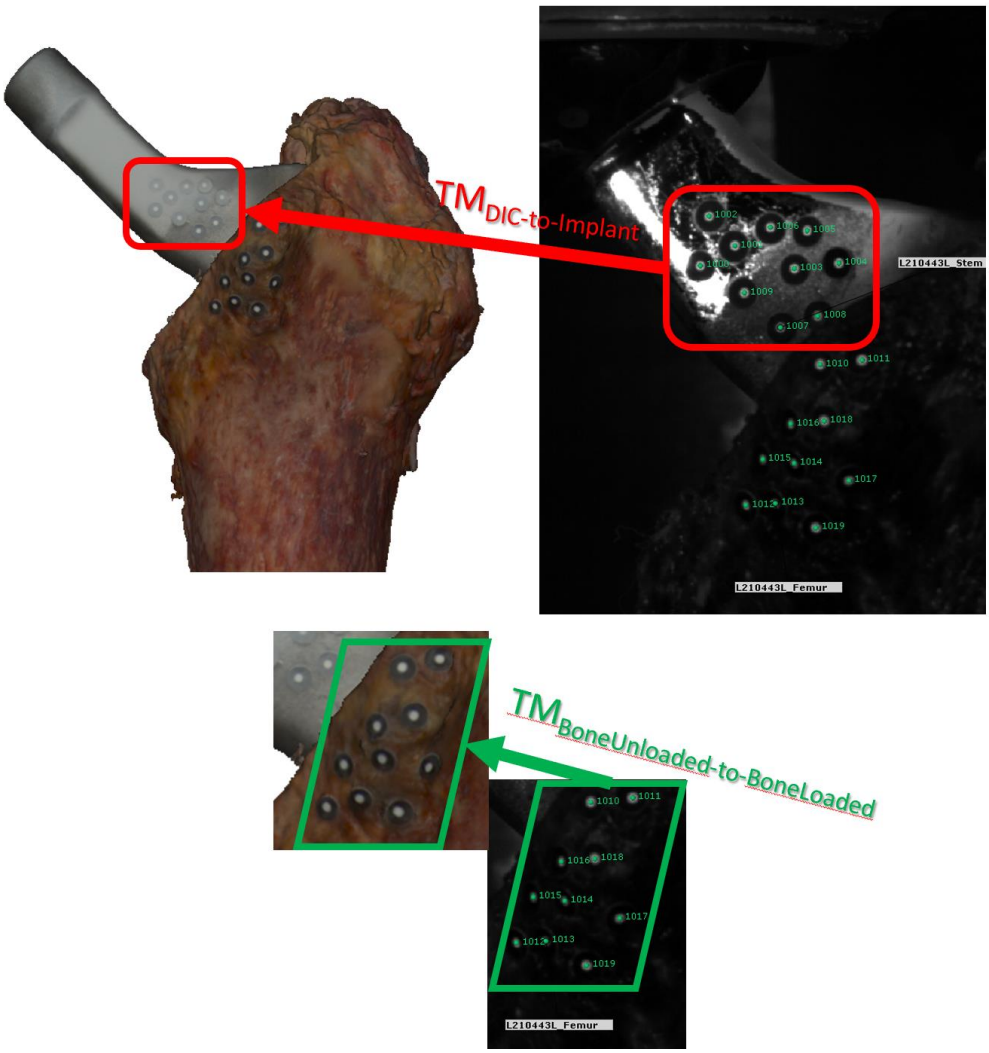

Figure 4.5 Flowchart of TMs to determine the final TM (TMBoneUnloaded-to-BoneLoaded) to determine Grood & Suntay kinematics of micromotion.

To estimate interface micromotions, the $TM_{BoneUnloaded\text{-}to\text{-}BoneLoaded}$ was applied to a dense regional mesh of the stem geometry localized to the stem-bone interface within 15mm of the calcar resection. Although femoral fixation of THA revision femoral stems occurs more distally in the femoral diaphyseal, this would have required creating windows in the shaft of the femurs that may have caused structural changes to the bone and thus influenced the micromotions seen. This proximal area of bone-implant interface was chosen as it was the closest area in which bony ingrowth would occur to the line-of-sight measurement area of the DIC. Micromotion was calculated for each node in the stem mesh in this proximal area by finding the displacement relative to the closest node on the femoral bony mesh through the cycle. The maximum micromotion was computed by calculating the maximum difference between the micromotion at any two time points during the cycle for each node. Cumulative displacement (integral of displacement over time) for each node during the different loading conditions were also calculated. Histograms of the bony interface area experiencing different levels of micromotion were calculated by binning the number of nodes that experienced increasing relative micromotion of 25 to 50μm bins, then normalized by the total number of nodes included in the interface mesh. The micromotion distributions were combined across specimens for each implant type to determine the mean and standard deviation of the percentage of nodes experiencing each magnitude of micromotion for each of the loading conditions.

The maximum torques and impactions were compared to the maximum micromotion for each of the specimen to determine if correlations existed. Micromotion from the 100% Gait loading conditions were used since micromotions were typically

largest during this test. The maximum impaction forces and maximum micromotion from 100% Gait loading were also compared to the sizes of each of the implants.

4.3 Results

The peak torque during the final reaming averaged 9.1Nm, with a range of 3.2 to 13.7Nm for the modular stem. The non-modular stem had an average of 11.9Nm, with a range of 8.9 to 15.9Nm (Figure 4.6).

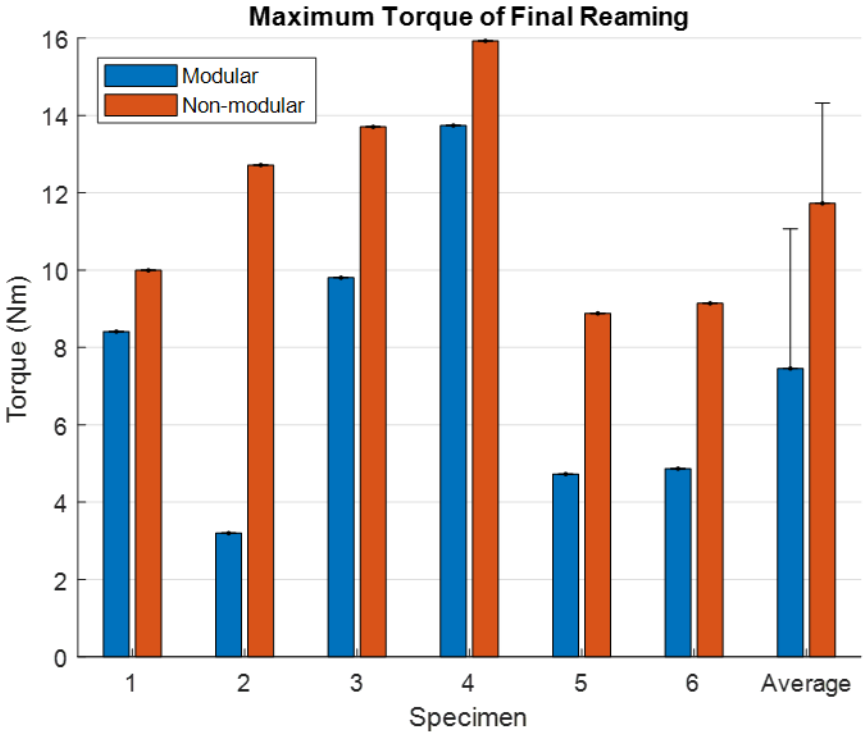

Figure 4.6 Maximum reaming torque found for the last reaming performed on each specimen.

The non-modular stems consistently required larger reaming torques when compared to the modular stem on the contralateral side. The paired sample t-test determined that the two implants had statistically different torques with a p-value of 0.0235 ($p<0.05$).

The final impaction force averaged 2784N, with a range of 1770N to 4610N for the modular stem. The non-modular stem had an average of 4378N, with a range of 1960N to 6400N (Figure 4.7).

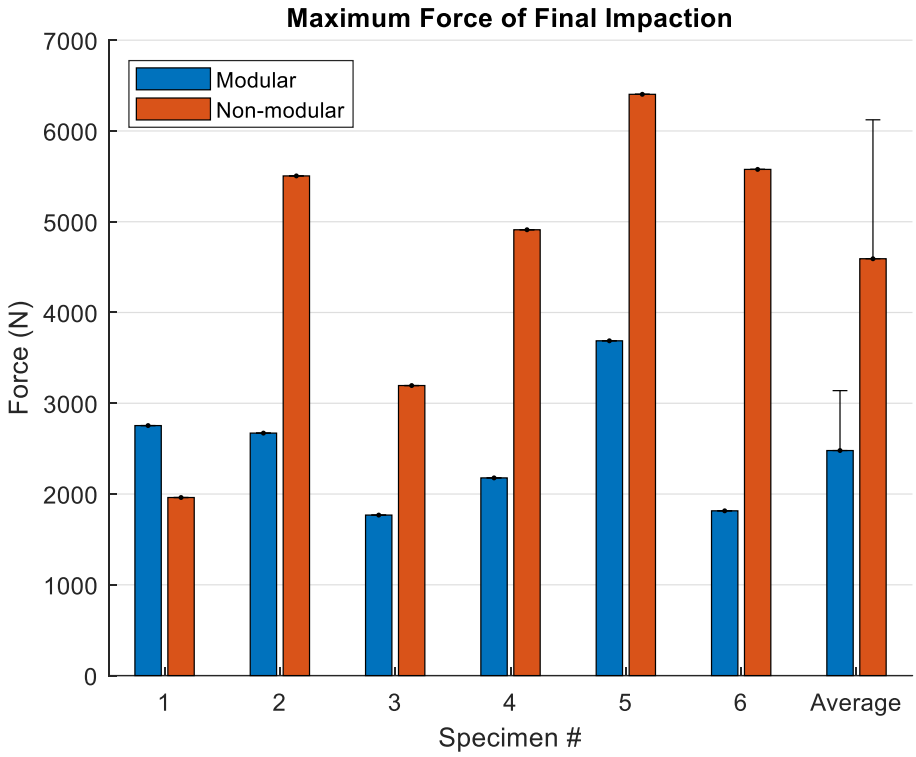

Figure 4.7 Maximum impaction force found for the last impaction performed that showed stem displacement on each specimen.

Similar to reaming torques, the non-modular stems had larger impaction forces compared to modular stems on the contralateral side, with the exception of Specimen 1. The paired sample t-test determined that the two implants had statistically different torques with a p-value of 0.0135 ($p<0.05$). The list of specimens with the corresponding implant type and size are shown in Table 4.2.

Table 4.2 Specimen List with Implant Type and Sizing

Specimen #	Specimen Number	Implant Type	Implant Size
1-Left	L210430L	Modular	17 w/ 20x85 Proximal Body
1-Right	L210430R	Non-modular	17
2-Left	L210435L	Modular	18 w/ 24x95 Proximal Body
2-Right	L210435R	Non-modular	18
3-Left	L210443L	Non-modular	16
3-Right	L210443R	Modular	16 w/ 20x85 Proximal Body
4-Left	S210681L	Non-modular	15
4-Right	S210681R	Modular	15 w/ 24x95 Proximal Body
5-Left	S211705L	Modular	15 w/ 20x85 Proximal Body
5-Right	S211705R	Non-modular	15
6-Left	S211834L	Modular	14 w/ 20x85 Proximal Body
6-Right	S211834R	Non-modular	14

Generally, the modular stem experienced equivalent or slightly larger movements compared to the non-modular stem, however, these differences were small and not statistically significant. For the simple AP loading, the mean difference in rotations was less than 0.05° and less than 0.05mm for translations (Figure 4.8). For the trapezoidal SI loading, the differences in rotations and translations were less than 0.04° and 0.05mm, respectively (Figure 4.9). During Gait, differences between modular and nonmodular stem were less than 0.1° for rotations and 0.03mm for translations (Figure 4.10). Stair Descent yielded similar results, with differences between modular and non-modular stems of 0.03° and 0.06mm, for rotations and translations respectively (Figure 4.11).

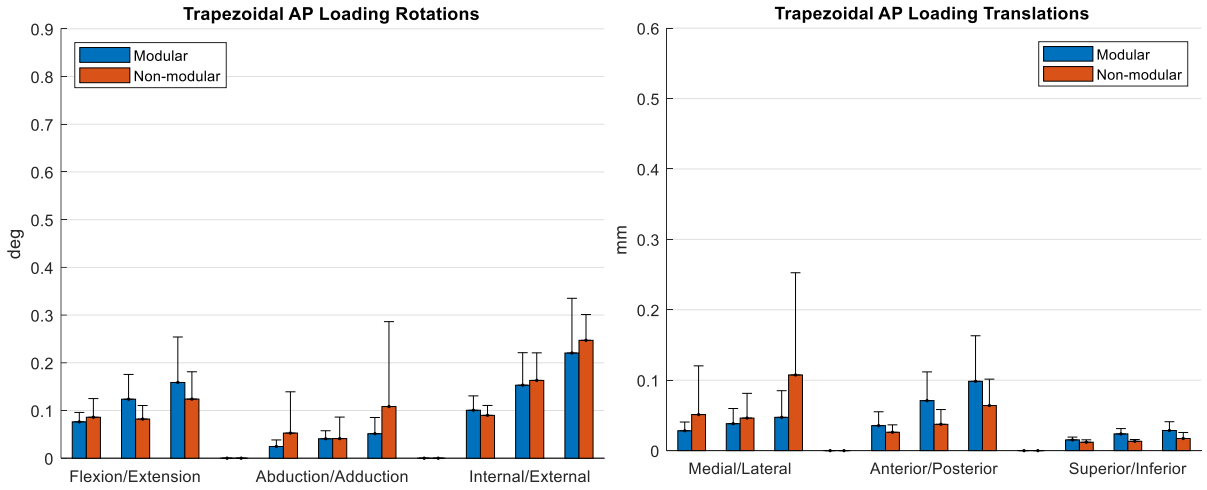

Figure 4.8 Kinematics for Trapezoidal AP loading, for increasing load of 50N, 100N, and 150N.

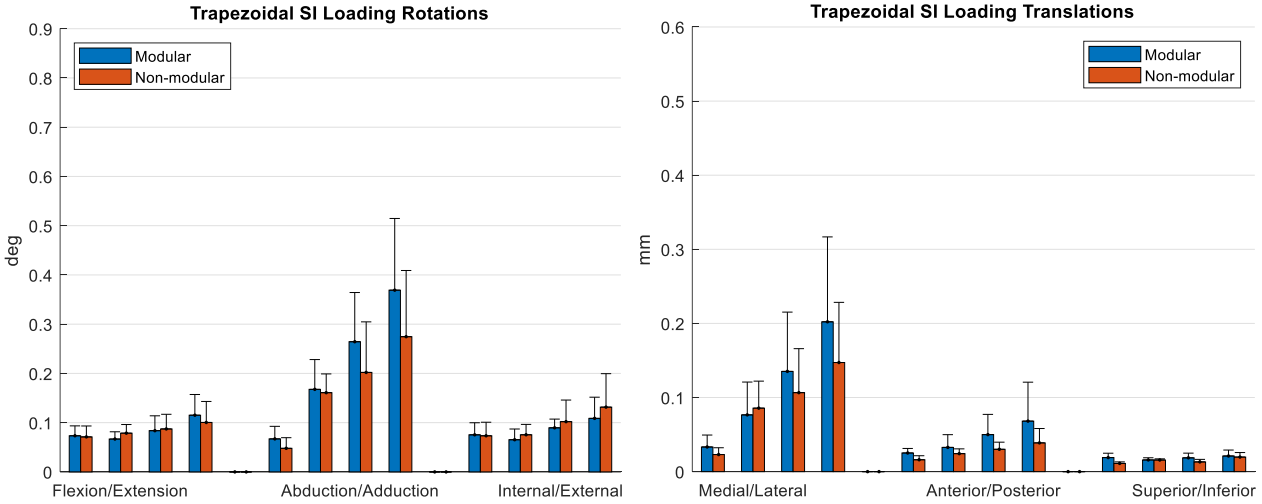

Figure 4.9 Kinematics for Trapezoidal SI loading, for increasing load of 400N, 900N, 1300N, and 1700N.

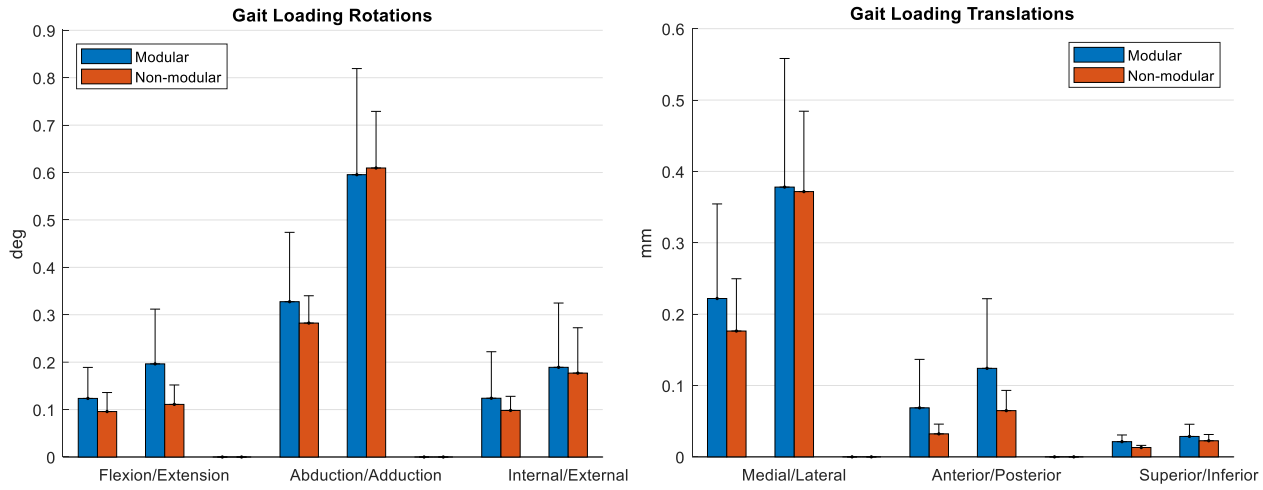

Figure 4.10 Kinematics for Gait loading conditions of 50% and 100%.

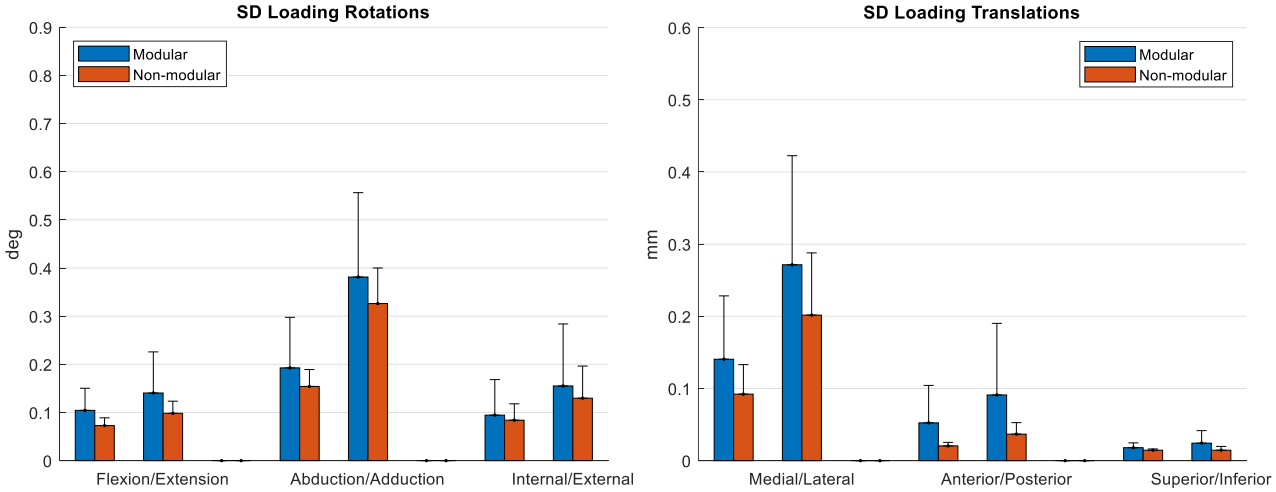

Figure 4.11 Kinematics for Stair Descent loading conditions of 50% and 100%.

As the amount of force applied in the simple AP and SI loading conditions increased, the amount of stem movement increased proportionally. The simple AP load applied to the femoral head created an I-E torque about the stem axis, which caused the dominant implant rotations to be about the I-E and F-E axes (Figure 4.8). Simple SI loading caused primarily adduction rotation and medial translation of the stem (Figure 4.9), which was the same dominant stem movement during gait and stair descent (Figures 4.10 and 4.11). The rotations and translations were higher in the activities of daily living than in the simple loading conditions. Specifically, the Ad-Ab rotations during the simple 150N AP loading was 0.05° and 0.10° for the modular and non-modular stems (Figure 4.8), and during the simple 1700N SI loading the Ad-Ab rotations were 0.35° and 0.28° (Figure 4.9). In contrast, Ad-Ab rotations during 100% Gait were greater than 0.60° for both stems designs (Figure 4.10), and for 100% Stair Descent were 0.38° and 0.32° for modular and non-modular stems, respectively (Figure 4.11). Similarly, M-L translations ranged from 0.1mm to 0.5mm during 150N AP loading (Figure 4.8), from 0.15mm to 0.2mm during 1700N SI loading (Figure 4.9), over 0.2mm for 100% Stair Descent (Figure 4.11), and nearly 0.4mm during 100% Gait (Figure 4.10). Similar changes were seen in the other kinematics, but were not as notable as abduction/adduction and medial/lateral translations.

The ANOVA conducted on the abduction/adduction and medial/lateral stem kinematics confirmed that the loading condition was the dominant factor in stem micromotions ($p<0.01$). No differences were observed between implant types ($p=0.446$). The Tukey's post-hoc showed that stem movement during 100% Gait was significantly

higher than the simple loading conditions ($p<0.05$), and similarly 100% Stair Descent was statistically greater from all loading conditions except 1300N and 1700N simple SI loads.

The distribution of micromotions across the stem-bone interface surfaces showed that the modular stem experienced higher micromotions than the non-modular stem (Figure 4.12). Specifically for the simple AP and SI loading, the modular stem had regions of the surface experiencing the highest micromotions, where the non-modular stem did not. Conversely, the non-modular stem had higher percentages of nodes in the lower ranges of micromotion compared to the modular stem (Figures 4.13, 4.14, 4.15, and 4.16). This same result was observed for Gait and Stair Descent, where the modular stem consistently had larger amounts of micromotion when compared to the non-modular stem (Figures 4.17 and 4.18). The surface micromotions during gait and stair descent produced larger amounts of micromotion compared to the simple AP and SI loading conditions. Specifically, during 150N AP loading, 42.5% of the surface experienced micromotions greater than 150μm for the modular stem and 10.2% for the non-modular stem (Figure 4.13 and 4.14). During 100% Gait, 96.3% of the surface experienced greater than 150μm for the modular stem, and 90.9% for the non-modular stem (Figure 4.17). During 100% Stair Descent, the 66.7% of the modular stem and 66.3% the non-modular stem had experienced greater that 150μm of micromotions (Figure 4.18).

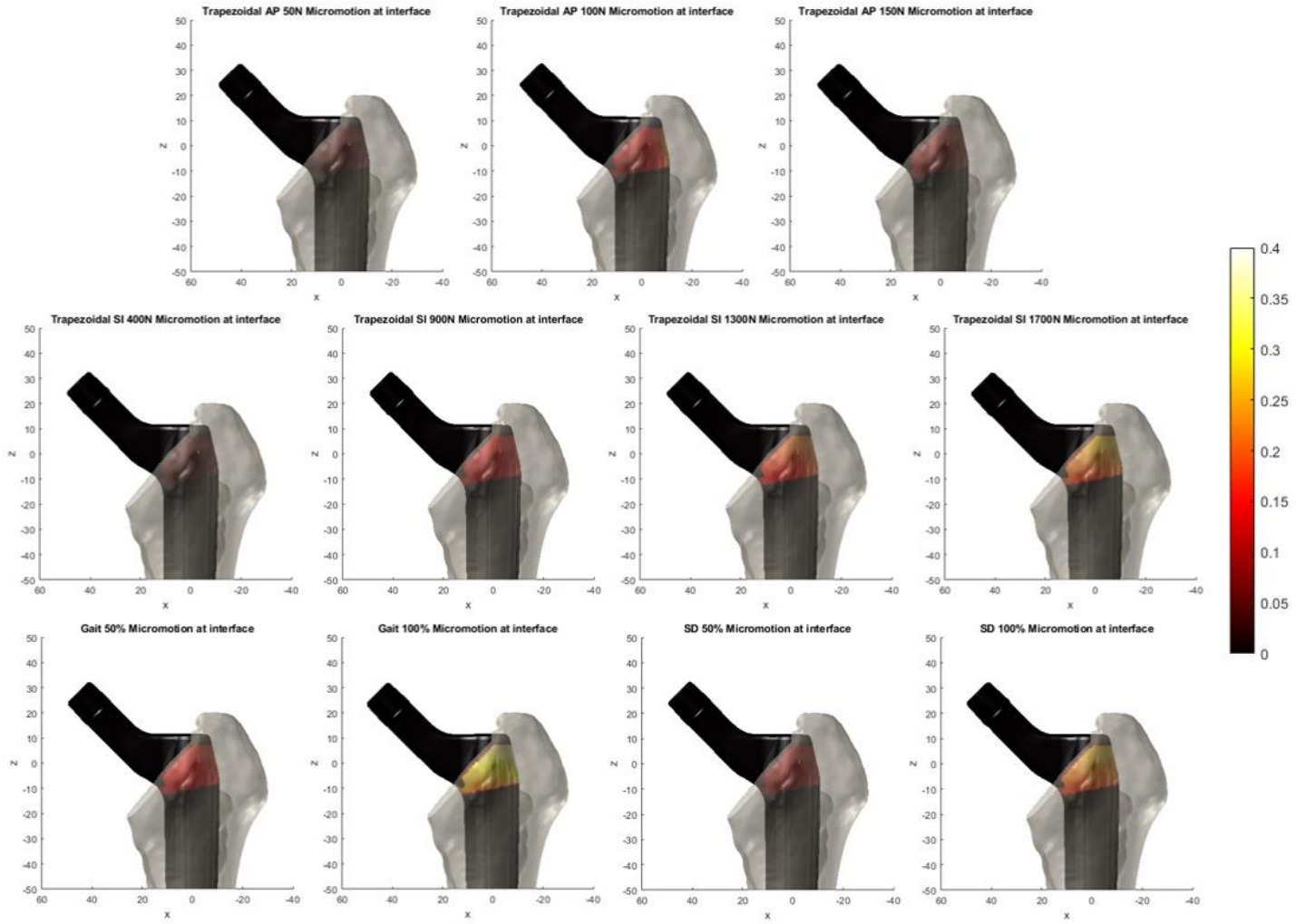

Figure 4.12 Visual comparison of changes in max micromotion at the bone-implant interface.

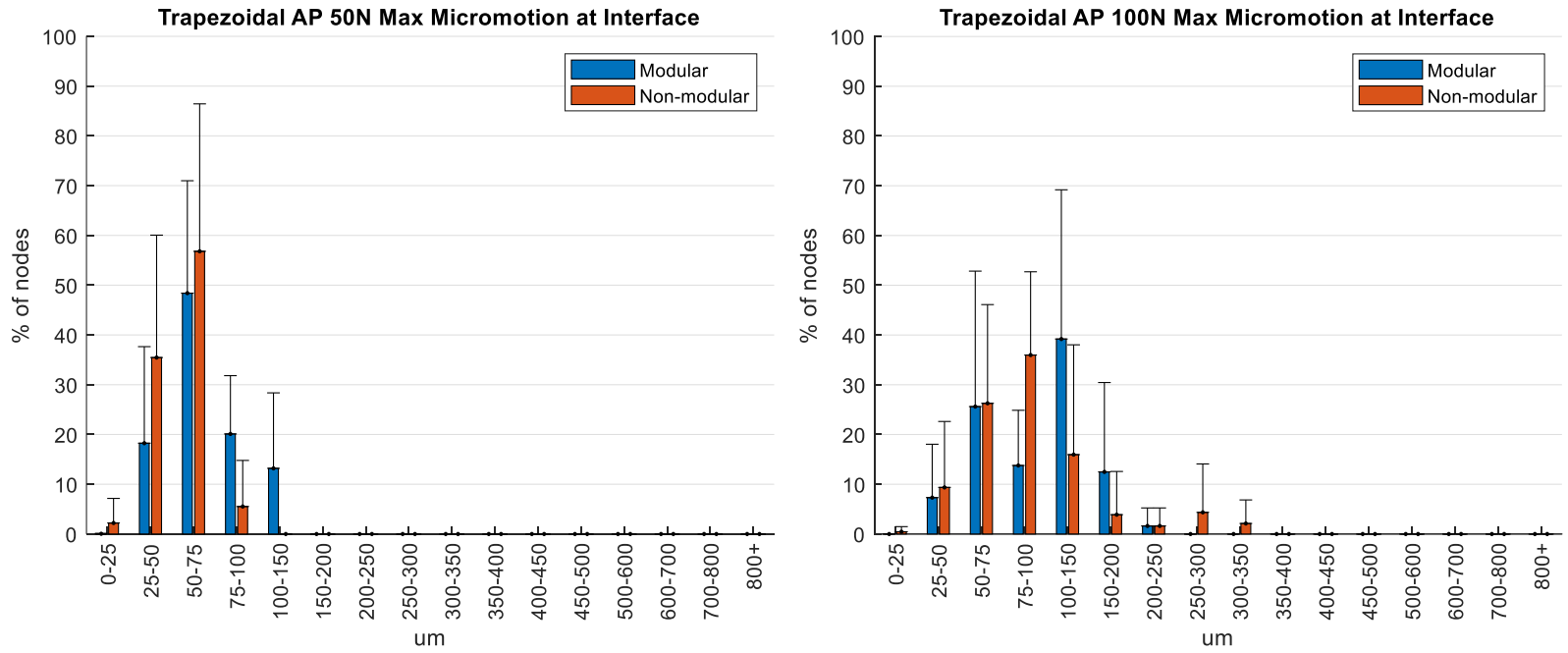

Figure 4.13 Bone-implant interface micromotion for simple Trapezoidal AP Loading for 50N and 100N.

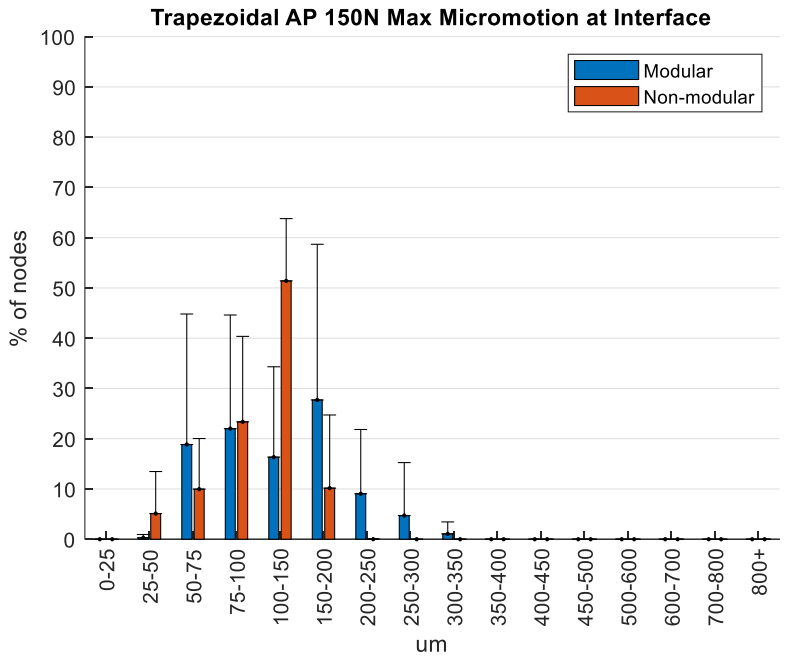

Figure 4.14 Bone-implant interface micromotion for simple Trapezoidal AP Loading for 50N and 100N.

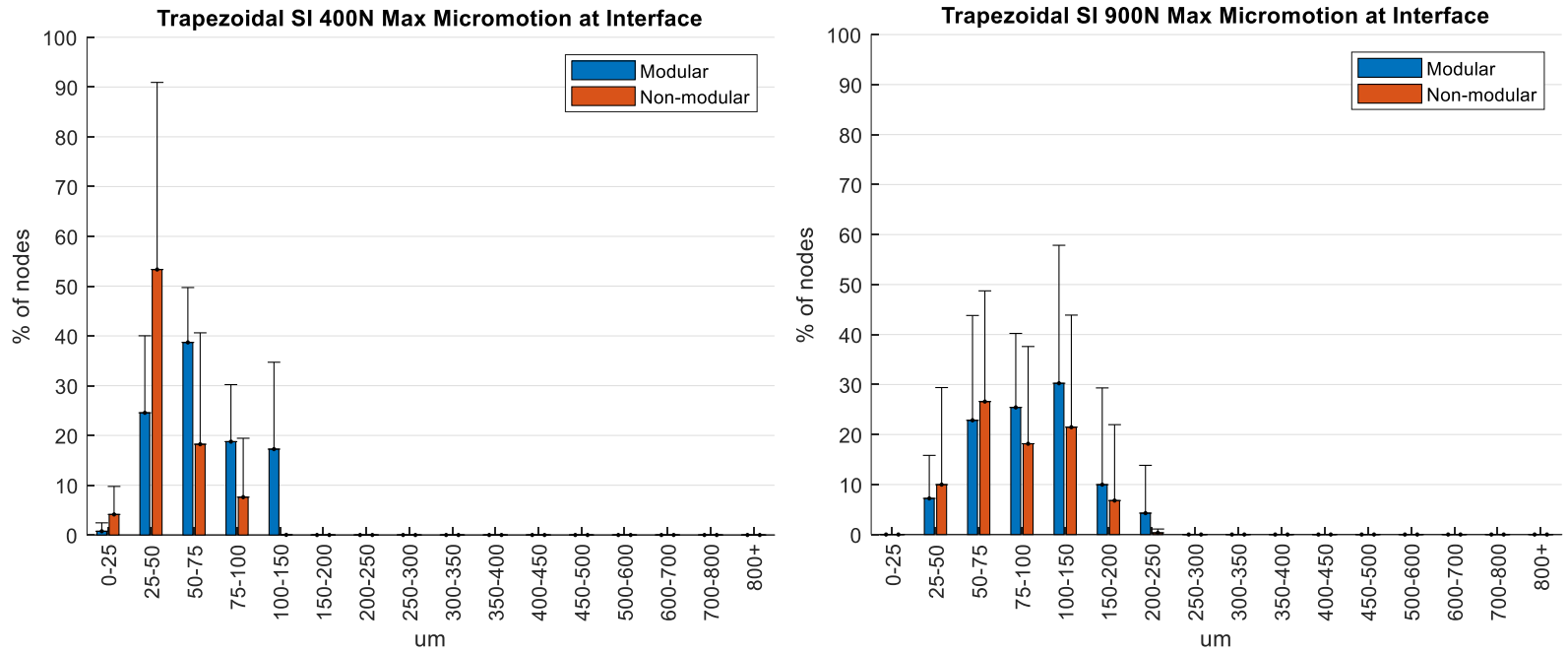

Figure 4.15 Bone-implant interface micromotion for simple Trapezoidal SI Loading for 400N and 900N.

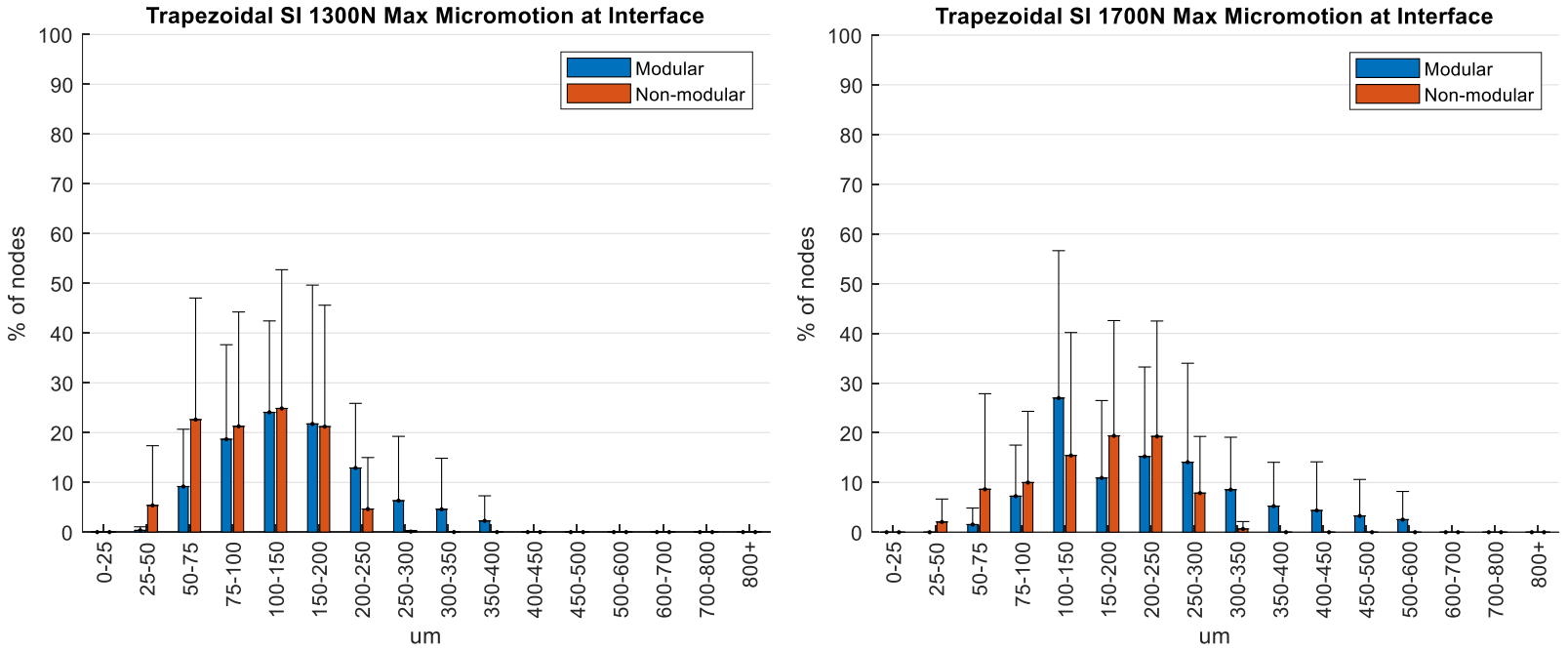

Figure 4.16 Bone-implant interface micromotion for simple Trapezoidal SI Loading for 1300N and 1700N.

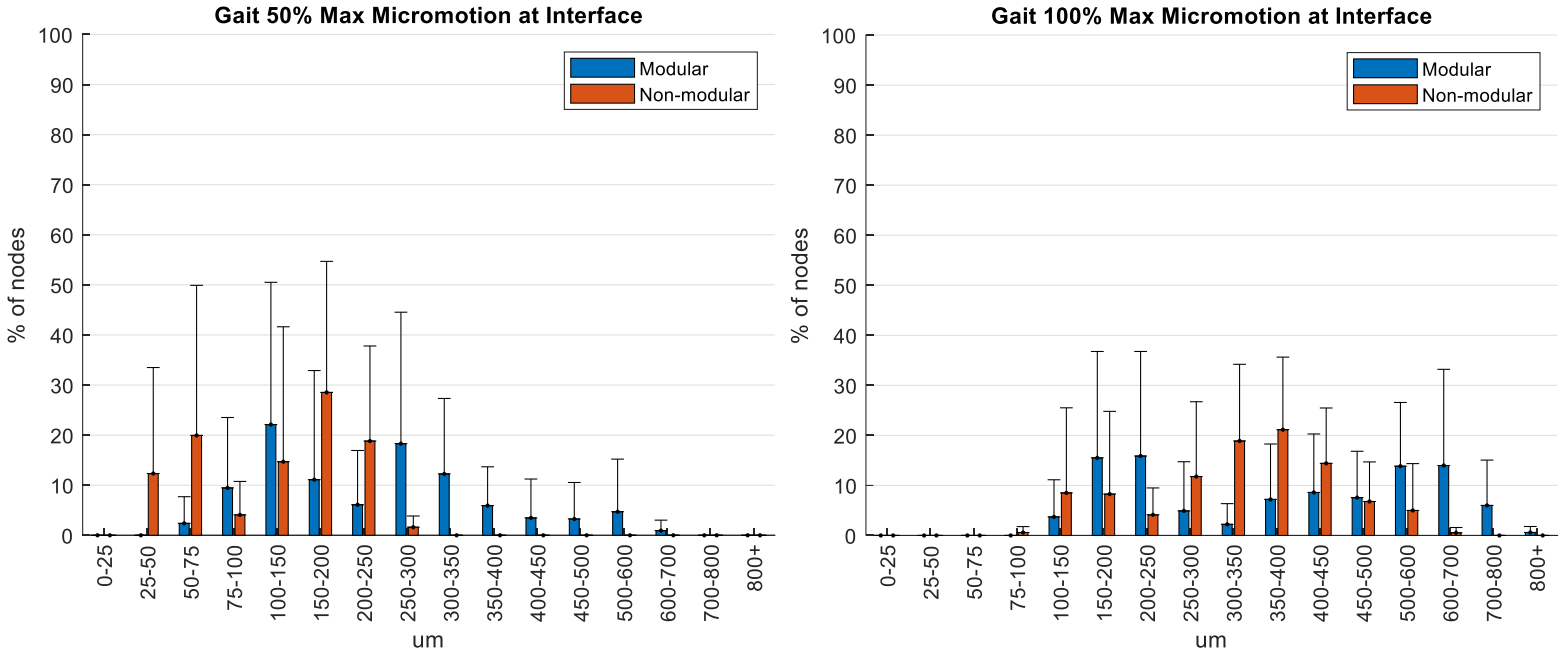

Figure 4.17 Bone-implant interface micromotion for Gait Loading conditions.

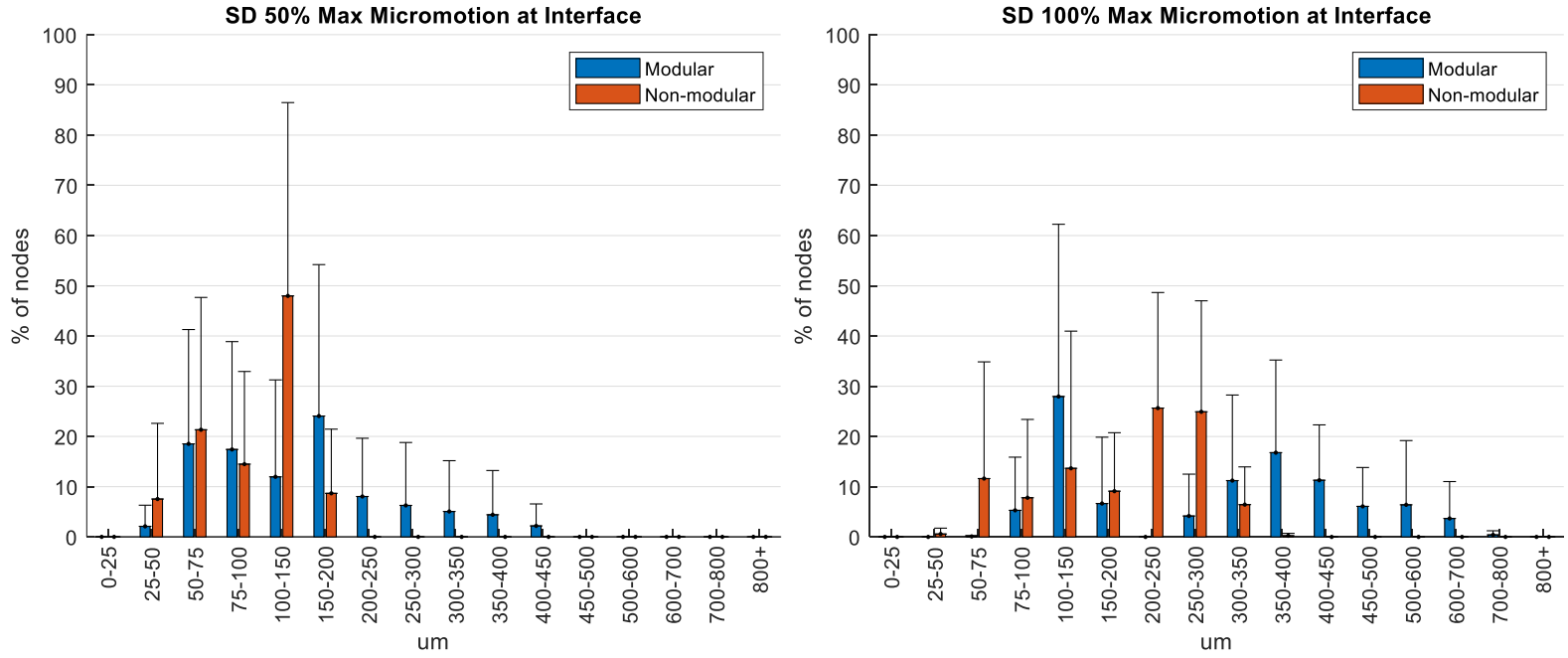

Figure 4.18 Bone-implant interface micromotion for Stair Descent Loading conditions.

No correlations were observed between the maximum reaming torque and the maximum micromotion, with an R^2 of 0.025 (Figure 4.19). Likewise, no relationship was observed between the maximum impaction force and the maximum micromotion with an R^2 of 0.021 (Figure 4.20).

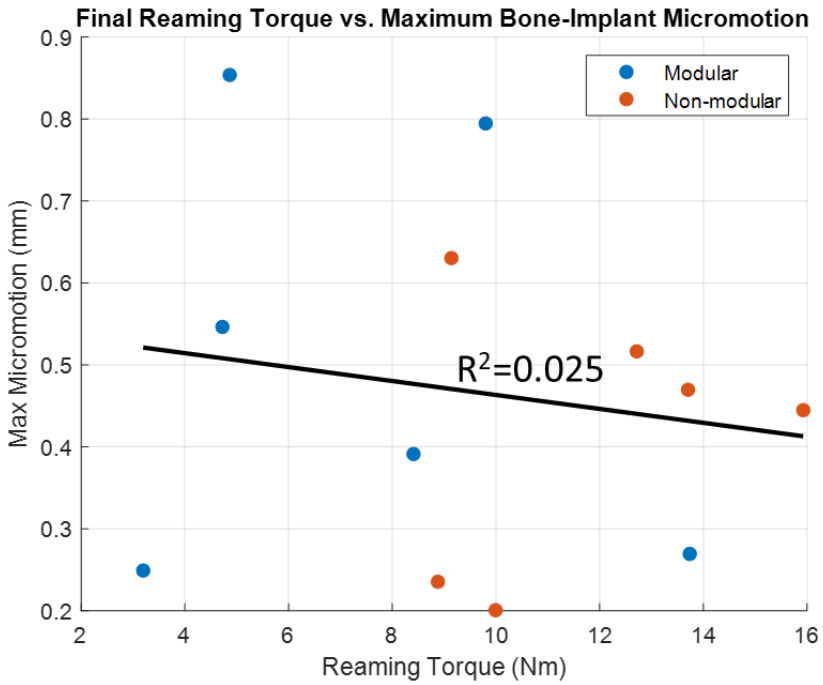

Figure 4.19 Comparison between the final reaming torque and the maximum micromotion seen at the bone-implant interface, with coefficient of determination (R^2).

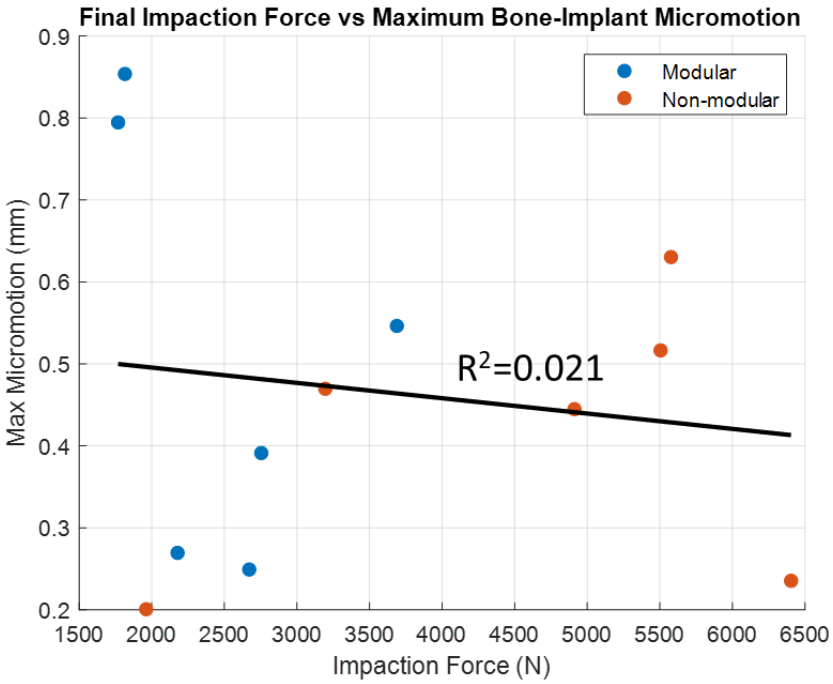

Figure 4.20 Comparison between the final impaction force and the maximum micromotion seen at the bone-implant interface, with coefficient of determination (R^2).

No correlations were observed between the size of the femoral stems and the maximum impaction forces, with an R^2 of 0.023 (Figure 4.21). Similarly, there was little to no relationship between the size of the stems and the maximum micromotion see with an R^2 of 0.179 (Figure 4.22).

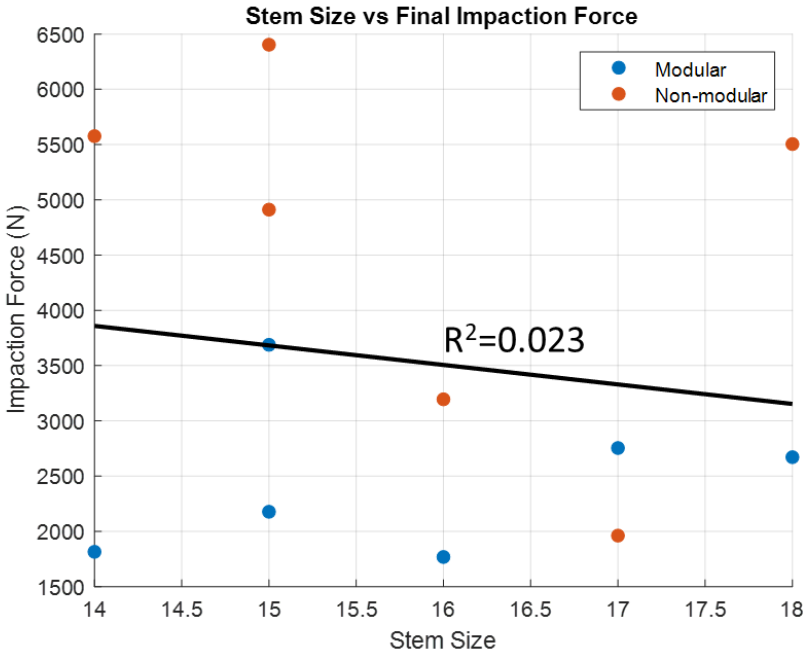

Figure 4.21 Comparison between the size of femoral stem and the final impaction force, with coefficient of determination (R^2).

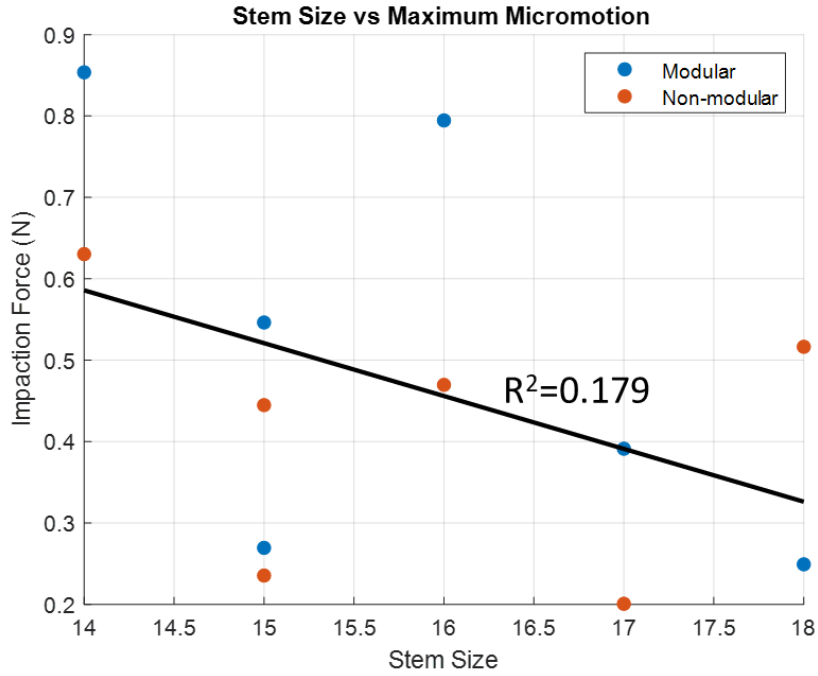

Figure 4.22 Comparison between the size of femoral stem and the maximum micromotion seen at the bone-implant interface, with coefficient of determination (R^2).

4.4 Discussion

The initial stability of cementless revision femoral stems is essential for the long-term success of revision THAs. Small amounts of micromotion are needed for osseointegration of the implant (Jasty et al., 1997). Many studies have looked at femoral stem micromotion, but have focused on simple loading conditions, instead of loading conditions from activities of daily living. These previous studies have focused on bone-implant interface micromotion instead of kinematics of the bone-stem movement. Due to these differences, comparison of micromotion magnitudes with other studies are difficult. Additionally, majority of studies focus on primary THA femoral stem fixation instead of revision femoral stems. One study found mean micromotion range from 37.4μm to 119.9μm for axial and torsional loading conditions respectively for the bone-implant interface (Camine et al., 2018), whereas another study found micromotions up to 91μm and 438μm (Small et al., 2017). Due to differences in experimental methodology and variation in loading conditions between previous literature, some comparisons can be made for the bone-implant interface micromotion, however, the greatest conclusions for revision THA femoral stem stability investigations are from within an individual study instead of interstudy comparisons. Primary THA femoral stems have higher rates of fixation proximally, whereas revision stems achieve better fixation distally in the diaphysis (Kwong et al., 2003). This study created bony voids in the femur before implantation to simulate a revision femoral stem procedure and to allow for more diaphyseal fixation distally in the femur.

Gait and Stair Descent loading conditions generated larger stem-bone movement when compared to the simple loading conditions, especially in abduction/adduction and medial/lateral translations. The ANOVA and Tukey's post-hoc tests show statistically significant differences in the loading conditions of the Gait and Stair Descent compared to the simple loads. This can be attributed to the activities of daily living loading conditions consisting of multiple dynamic loading conditions in AP, ML, and SI, versus the simple loading conditions of one trapezoidal loading condition applied to the femoral stem. These statistical tests showed that there was no statistically significant difference between the type of implant (modular and non-modular).

The bone-implant interface micromotion showed smaller amounts of micromotion in the simple loading conditions of the AP and SI loading when compared to Gait and Stair descent. It can specifically be seen that the maximum amount of micromotion reached by any node along the interface for the simple loading conditions was up to 600μm, but were centered near the 150μm area (Figures Figures 4.13, 4.14, 4.15, and 4.16). Gait and stair descent reached micromotions upwards of 800μm, with an average closer to 300μm (Figures 4.17 and 4.18). These results help confirm the hypothesis that realistic loading conditions will cause larger amounts of micromotion when compared to that of simple loading conditions. Previous studies have focused on bone-implant interface micromotion instead of kinematics of the stem-bone movement. Small et al measured micromotion up to 438μm for a non-modular stem along the proximal portion of the bone-implant interface under an axial load of 1675N and an axial torque of 20Nm (Small et al., 2017). This can be compared similarly to the results of the 1700N SI load in

the current study that produced micromotions up to 300μm for the non-modular stem and up to 600μm for the modular stem (Figures 4.15 and 4.16). Ong et al compared short versus long stem femoral implants and found micromotions up to 112μm for 45% Gait loading and up to 727μm for Stair Climbing (Ong et al., 2009). This study resulted in micromotions up to 300μm for non-modular and up to 700μm for modular stems during 50% Gait loading (Figure 4.17). For stair descent, the non-modular stem experienced up to 350μm of micromotion and modular experienced up to 750μm (Figure 4.18). Although these studies show similar magnitudes in micromotions, these studies were performed on primary THA femoral stems versus revision femoral stems. The previous studies support that micromotions are greater in activities of daily living versus simplified loading conditions.

In this study, the stem-bone movement was measured on exposed surfaces in the line-of-sight of the DIC camera system where no bony on-growth will ever occur. We necessarily assume that stem-bone interface micromotions are proportional to the observed micromotion at the exposed surfaces. Measurement of micromotion near the femoral diaphysis, where fixation of revision stems would typically occur, would have required creating a window on the distal portion of the femur to view the movement of the stem distally and caused structural damage to the bone that could influence this fixation. Continued work for this study includes verification of Finite Element (FE) models of the bone-implant constructs in this experiment to predict interface micromotions and determine correlations between DIC and FE measures. More specifically, the finite element models will be used to analyze differences in micromotion

measured proximally to those predicted to occur distally where primary fixation with the diaphyseal bone is expected. Magnitudes of micromotion may differ between the experimental and computational methods, but the use of the combined methods are necessary to gain a better understanding of the micromotion seen of the femoral stem relative to the femur.

This study had some limitations in the methodology. This study does not account of time-dependent bone remodeling, and thus is a representation of an initial postoperative femur. Additionally, the loading conditions were based upon an averaged 75kg specimen tested from Orthoload. Patient's weight varies greatly in clinical practice, and thus the loading conditions would be different for other patients, thus the results may be larger than individuals who have smaller weights, especially for the smaller implant sizes tested. Vice versa, the amount of micromotion may increase for patients with a larger weight. Future work should consider scaling the loading conditions based upon bone size or specimen weight.

The findings of this study suggest that micromotion studies for cementless revision femoral stems need to include loading conditions from activities of daily living in order to accurately calculate the amount of initial micromotion and stability of the stem. The results showed that the activities of daily living caused larger amounts of micromotion than the simple loading conditions did. The use of simple loading conditions may be used to compare the micromotions between two or more designs, but future studies should include activities of daily living loading conditions, not just limited

to Gait and Stair Descent, to accurately determine femoral stem micromotion for the safety of a single design.

Chapter Five: Accuracy Tradeoffs between Individual and Joint-Level Statistical Shape Models of Knee Morphology

5.1 Introduction

Anatomic variation is an important consideration when assessing pathology, planning surgical interventions, and designing orthopaedic implants and devices. Statistical shape models (SSM) are commonly used to quantify variation in the anatomy of the bone and soft tissue structures (Goparaju et al., 2022, Taylor et al., 2013). SSM models have also been used to characterize variability in the population (Mahfouz et al., 2012) and to support implant sizing (Dai et al., 2014, Fitzpatrick et al., 2011). SSMs are able to build virtual populations, that can then support product design and evaluation, for example, Galloway et al. generated virtual subjects considering shape, material property and joint load variation (Galloway et al., 2013). Workflows to create personalized instances have also been used to support surgical planning (Bruse et al., 2017) and biomechanical modeling (De Roeck et al., 2021). Early SSMs quantified variation in an individual bone, including femur models to assess shape variability in patients with hip dysplasia (Gaffney et al., 2019). Individual bone SSMs have also included the modeling of the pelvis to develop automatic CT data segmentation (Seim et al., 2008) and modeling of the humerus to investigate the differences ethnicity and gender have on the morphology of the bone (Sintini et al., 2018). This work focuses on the knee joint, specifically on the femur and tibia. Pedoia et al., 2015 developed a statistical shape model

of the femur and tibia from MR and investigated differences between have looked at modeling each bone within the knee individually and analyzed shape differences specifically to each bone (Pedoia et al., 2015). Other studies have developed individual bone SSMs of the knee and analyzed the correlation in changes of the shapes to one another (Wise et al., 2016). Recent efforts have grown to capture variation in multiple structures of a joint, including the bony anatomy and soft tissue structures (e.g. cartilage, and ligament attachments). Some studies have developed the SSM around the knee joint to specifically look at shape variations of the joint as a whole (Cerveri et al., 2020) or to analyze changes in contact areas of the joint (Rao et al., 2013). However, there are virtually no studies that compare the accuracy between individual and joint level SSMs.

Accuracy of SSMs has often been assessed by quantifying how much variation is captured in a specified number of early modes, errors computed in a leave-one-out evaluation, and a parallel analysis to assess potential noises (Horn, 1965). Recently, Audenaert et al., 2019, recommended evaluations of accuracy, compactness, generalization, and specificity. The accuracy measure was used to analyze how well bony models or subjects are captured with different amounts of variation within the model. Compactness was determined by the cumulative explained variance in the model. The generalization measure was a leave-one-out analysis, that was used to quantify the ability of the SSM model to represent new shape instances. Lastly, specificity measured the realistic ability of the SSM to develop new random shape instances (Audenaert et al., 2019).

The objective of this study was to assess tradeoffs in accuracy between SSMs describing an individual bone and SSMs of the knee joint versus SSMs of the femur or tibia individually. Specifically, to perform this evaluation, SSMs were developed for matched pairs of femurs and tibias and evaluations compared the predictive ability of joint-level and individual bone models, utilizing the measures outlined by Audenaert et al., 2019. The secondary objective of this study was to repeat these measures with the same SSMs that have had the meshes decimated by 50%. This study hypothesized that individual bone models will produce more accurate results due to these measures. This study also hypothesized that the full mesh would result in higher accuracy than the 50% decimated mesh according to these measures.

5.2 Methods

Preoperative CT scans containing the distal femur and proximal tibia were segmented into 3D models for 179 TKA patients (108 female and 71 male, 115 Caucasian and 64 Asian) with osteoarthritis prior to undergoing a total knee arthroplasty (TKA) procedure (Table 5.1).

Table 5.1 Demographic information on the training set.

Ethnicity	**Female**	**Male**	**Total**
Caucasian	76	39	115
Chinese	17	27	44
Japanese	15	5	20
All Ethnicities	108	171	**179**

Data was deidentified for use in this study and classified as exempt by the DU institutional review board. An anatomical coordinate system was established for an average-sized bone geometry, which served as the template. The data set was duplicated, with on staying at full mesh density and the other set was decimated by 50%. The full mesh femur had 49767 nodes with an average edge length of 0.83mm and tibia had 20296 nodes with a edge length of 0.95mm. The 50% decimated mesh for the femur had 24884 nodes with an average edge length of 1.26 mm and the tibia had 10149 nodes with an edge length of 1.48 mm.

To establish correspondence, each bone was registered independently to the corresponding template using rigid iterative closest point (ICP) and non-rigid coherent point drift (CPD) techniques (Besl et al., 18, Myronenko et al., 2010). Both methods iterate through each of the nodes in the template mesh of the bone and matches it to the closest node in the mesh for each training set subject. The ICP algorithm carried out a rigid body alignment, where the position and rotation of the instance was optimized to reduce the Euclidean or root mean square error summed for all of the nodes. To better capture shape variations between template and instance, the deformable CPD algorithm was employed used the nonrigid low-rank method with a max number of 100 iterations and a tolerance of 1e-6. Next, principal component analysis was applied to the established register of nodal coordinates. SSMs were developed for the individual bone and the overall joint, resulting in three SSMs: Femur-only, Tibia-only, and Joint-level (femur and tibia).

The emphasis of this study is on evaluating differences between the individual and joint-level SSMs, and the following measures were assessed: compactness, accuracy, generalizability, and specificity (Audenaert et al., 2019).

The evaluation of Compactness used the percentage of variation explained by each of the modes as derived from the principal component analysis. The percentages were summed to represent cumulative variation and plotted against the number of modes. Compactness was computed and compared for Femur-only, Tibia-only, and Joint-level SSMs.

Accuracy, which evaluates the ability of the model to describe the training set, is computed as the average ± standard deviation for each member of the training set and evaluated for a specific number of PC modes included. A common approach is to employ the number of PC modes that correspond to characterizing 95% of the variation, noting this number of modes varies for the Tibia-only, Femur-only and Joint-level SSM. The specified number of modes were used to create a predicted instance and then error comparing the predicted and original geometry was computed. When all modes are included, the predicted instance will be identical to the original geometry and the error will be 0.

Generalization involves a leave-one-out analysis, which assesses the ability of the individual bone and Joint-level SSMs to represent an unseen subject. With each subject left out, an SSM was constructed based on the remaining subjects and principal component (PC) scores were computed to predict the geometry of the left-out subject using a specified number of modes. Errors were computed as the Euclidean distance

between corresponding nodes of the SSM-predicted and actual geometries. Mean geometric errors for the subjects were captured in box plots for each SSM prediction and with the varying number of modes. Overlay plots were developed to highlight the differences for max and mean error subjects using the number of modes that correspond to 95% variation explained. These processes were repeated for Femur-only, Tibia-only, and Joint-level SSMs.

Specification was computed to predict the ability of the SSM to predict random new geometries, by conducting a PC analysis on the model and computing the standard deviations for each of the PC scores found. These standard deviations were randomized and applied to create a completely random subject instance. This randomized subject was iterated through all 179 subjects to find the closest original geometry to the random instance, by computing the RMSE for each node. The average error and standard deviation of the error between the randomized subject and the closest original geometry were computed. This was repeated a total of 1000 times. This process was repeated for the Femur-only, Tibia-only, and Joint-level SSMs.

To explore the sensitivity of these measures to mesh density, all of these measures were evaluated for SSMs based on the original mesh and with a 50% decimated mesh.

5.3 Results

The amount of variation described in the early modes differed between the individual bone and Joint-level SSMs, as computed from the Compactness measure (Figure 5.1).

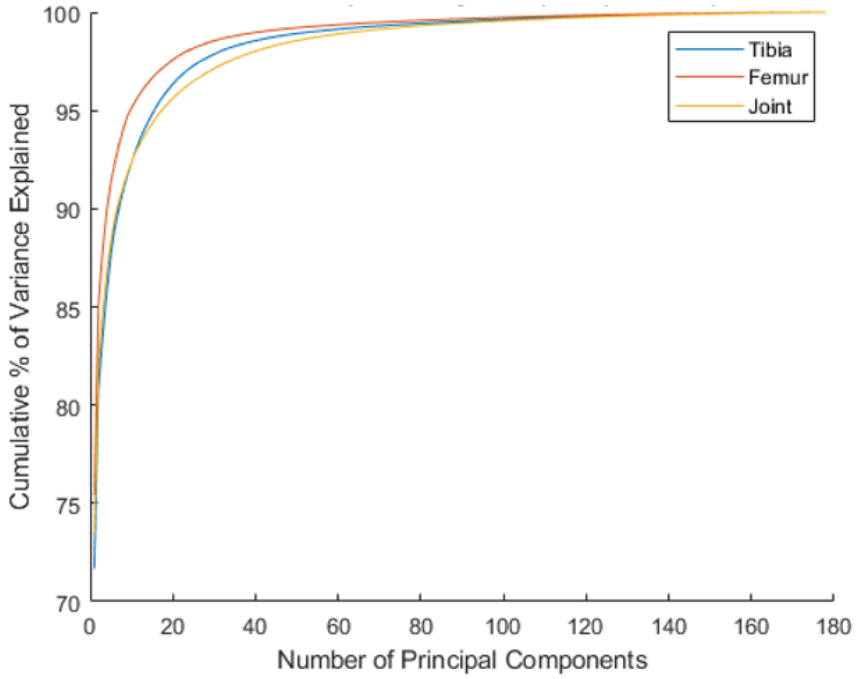

Figure 5.1 Plot of compactness measure showing the increase in cumulative variance explained as the number of principle components increase.

In the Full Mesh evaluation, for the Femur-only SSM, 10 modes captured 95.1% of the geometric variation with mode 1 describing 75.4%, while for the Tibia-only SSM, 16 modes captured 95.2% of variation with mode 1 describing 71.7%. In the Joint-level SSM, 18 modes captured 95.2% of variation with mode 1 describing 73.5% shown in Table 5.2.

Table 5.2 Compactness results for each of the SSMs for both full mesh and 50% decimated mesh. Brackets denote results with modes corresponding to 95% variation explained.

	Full Mesh (Percentage Explained)			**50% Decimated Mesh (Percentage Explained)**		
# of Modes	**Femur**	**Tibia**	**Joint**	**Femur**	**Tibia**	**Joint**
1	75.43	71.69	73.46	74.34	68.05	72.21
2	85.09	80.79	82.09	82.56	77.15	79.54
3	87.81	83.41	84.65	86.04	80.55	82.91
4	89.85	85.67	86.70	88.39	83.19	85.06
5	91.31	87.62	88.33	90.11	85.22	86.62
10	[95.12]	92.34	92.36	94.34	90.86	91.17
12	95.84	93.50	93.27	[95.17]	92.19	92.21
16	96.88	[95.19]	94.65	96.40	94.30	93.80
18	97.25	95.82	[95.17]	96.83	[95.05]	94.12
20	97.58	96.35	95.62	97.21	95.69	[94.94]
30	98.55	97.87	97.13	98.32	97.48	96.70
40	98.97	98.55	98.02	98.81	98.27	97.71
50	99.21	98.92	98.55	99.08	98.69	98.33
60	99.36	99.14	98.90	99.26	98.96	98.72
80	99.58	99.43	99.31	99.51	99.32	99.22
100	99.74	99.63	99.57	99.69	99.56	99.50
178	100	100	100	100	100	100

More modes were required in the joint-level model to capture the same amount of variation in an individual bone model. This finding was also observed for the 50% reduced mesh.

The first three modes of the SSMs for the Femur and Tibia are shown in Figure 5.2. In both bones, Mode 1 primarily described scaling. Mode 2 for the Femur described changes in condylar shape, particularly in medial-lateral width. Changes in Mode 2 for the Tibia corresponded to non-uniform scaling of the condyles, particularly in medial-

lateral and internal-external rotations, as well as changes at the tubercle. Mode 3 for the Femur captured medial-lateral rotation (posterior slope) and changes of the relative positioning of condyles and shaft. Mode 3 of the Tibia described changes at the tubercle, plateau, and shaft that creates a posterior overhang.

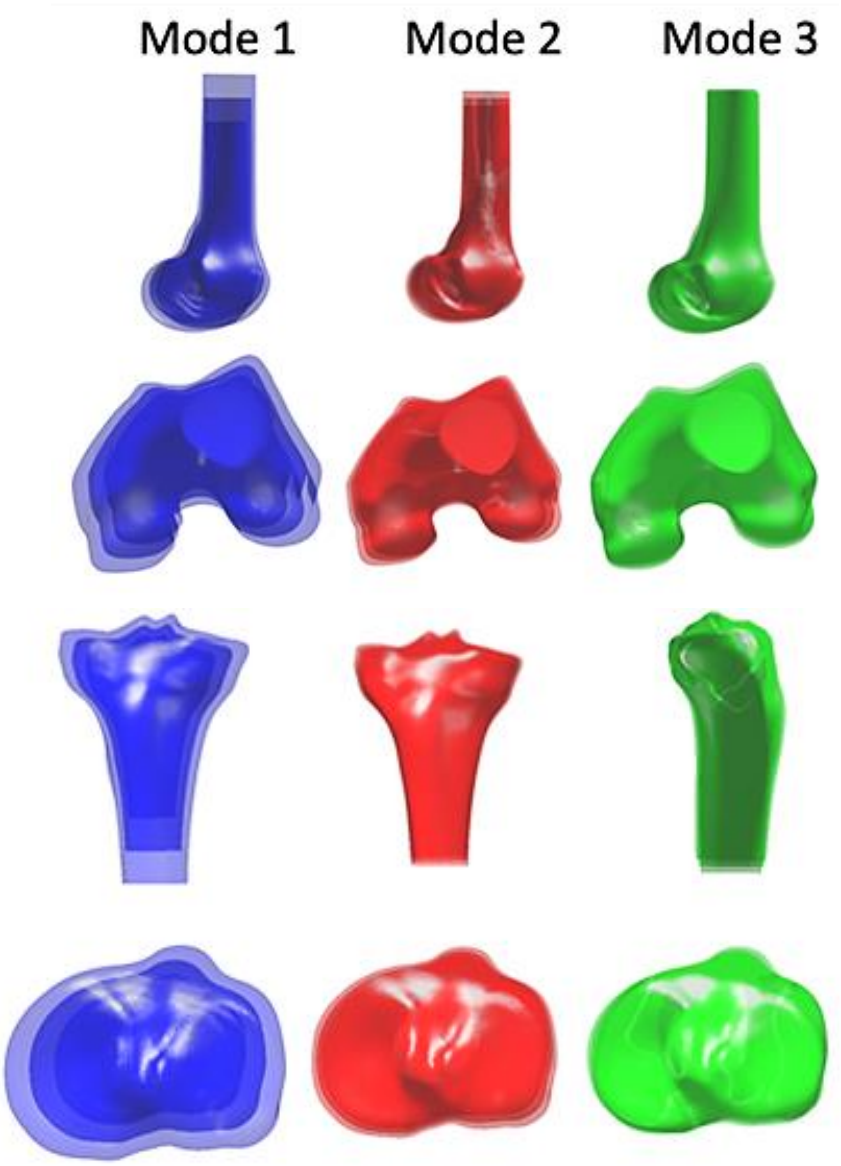

Figure 5.2 Visualization of first three modes of Femur and Tibia SSMs.

Accuracy resulted in plots showing the change in the error as more modes were included, which resulted in a decrease in the error as the number of modes increased for Femur-only and Tibia-only SSMs, as well as for the Joint-level SSM (Figure 5.3).

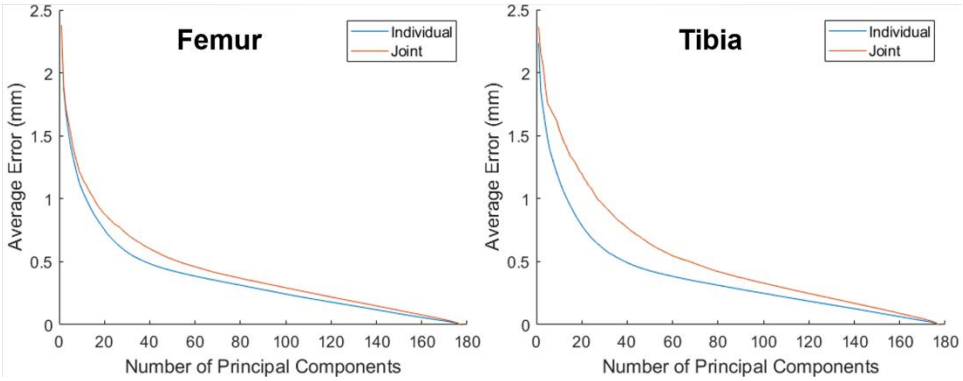

Figure 5.3 Plots of Accuracy comparison between individual bone SSMs and Joint level SSM for the Femur and Tibia.

Using the same number of modes, accuracy for the individual bone SSMs were consistently smaller than for the joint models, and this was observed for both the full mesh and the 50% decimated mesh (Table 5.3).

Table 5.3 Accuracy results for each of the SSMs for both full mesh and 50% decimated mesh. Brackets denote results with modes corresponding to 95% variation explained.

Full Mesh Error (mm)				
# of Modes	**Femur-only**	**Joint level (Femur)**	**Tibia-only**	**Joint level (Tibia)**
10	[1.08 ± 0.19]	1.18 ± 0.19	1.15 ± 0.22	1.54 ± 0.29
12	0.99 ± 0.17	1.11 ± 0.18	1.06 ± 0.20	1.45 ± 0.27
16	0.86 ± 0.14	0.98 ± 0.16	[0.91 ± 0.15]	1.32 ± 0.24
18	0.80 ± 0.13	[0.92 ± 0.15]	0.84 ± 0.14	[1.30 ± 0.22]
20	0.75 ± 0.12	0.88 ± 0.14	0.79 ± 0.13	1.20 ± 0.20
All	0.0 ± 0.0	0.0 ± 0.0	0.0 ± 0.0	0.0 ± 0.0
50% Decimated Mesh Error (mm)				
# of Modes	**Femur-only**	**Joint level (Femur)**	**Tibia-only**	**Joint level (Tibia)**
10	1.09 ± 0.19	1.20 ± 0.21	1.17 ± 0.23	1.54 ± 0.28
12	[1.01 ± 0.17]	1.11 ± 0.17	1.08 ± 0.22	1.48 ± 0.27
16	0.87 ± 0.15	0.99 ± 0.16	0.92 ± 0.16	1.27 ± 0.23
18	0.81 ± 0.14	0.93 ± 0.15	[0.88 ± 0.14]	1.27 ± 0.22
20	0.76 ± 0.13	[0.88 ± 0.14]	0.80 ± 0.13	[1.21 ± 0.20]
All	0.0 ± 0.0	0.0 ± 0.0	0.0 ± 0.0	0.0 ± 0.0

Generalization resulted in the box plots that showed the change in error based upon the iterated number of modes for the full mesh in Figure 5.4 and the 50% decimated mesh in Figure 5.5. The comparison between the two mesh sensitivities is also shown numerically in Table 5.4.

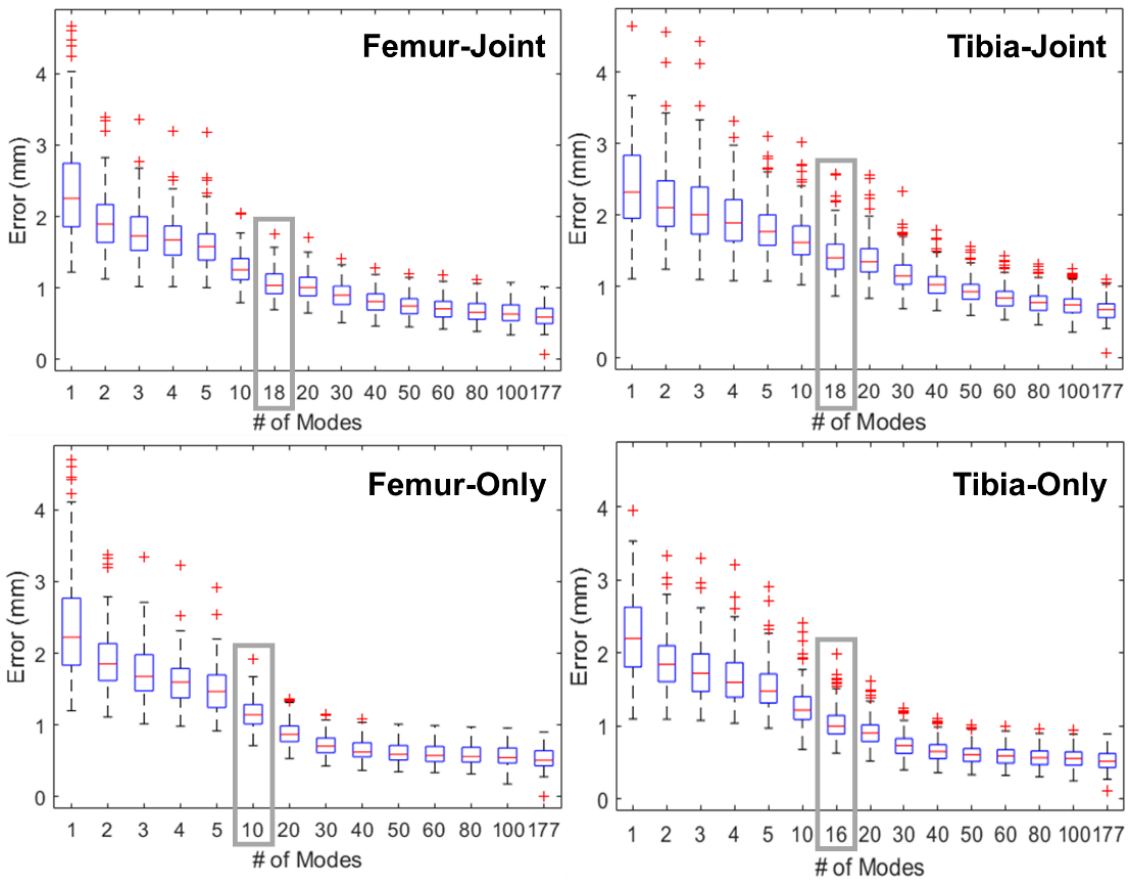

Figure 5.4 Plots of generalization measure for the full mesh that show the averages, standard deviations, and outliers for each SSM with increasing number of modes applied.

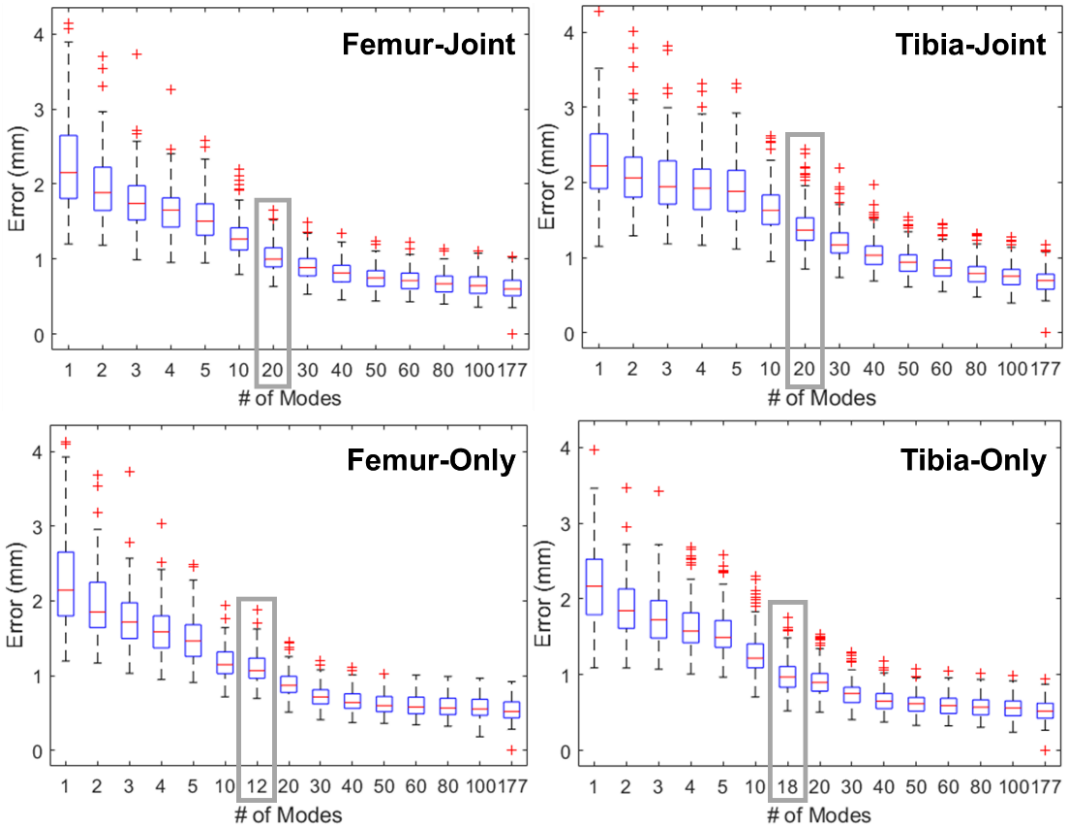

Figure 5.5 Plots of generalization measure for the 50% decimated mesh that show the averages, standard deviations, and outliers for each SSM with increasing number of modes applied.

Table 5.4 Generalization results for each of the SSMs for both full mesh and 50% decimated mesh. Brackets denote results with modes corresponding to 95% variation explained.

Full Mesh Error (mm)				
# of Modes	**Femur-only**	**Joint level (Femur)**	**Tibia-only**	**Joint level (Tibia)**
10	[1.16 ± 0.21]	1.27 ± 0.23	1.26 ± 0.28	1.67 ± 0.33
12	1.09 ± 0.20	1.22 ± 0.22	1.17 ± 0.26	1.60 ± 0.32
16	0.97 ± 0.18	1.11 ± 0.21	[1.04 ± 0.22]	1.48 ± 0.30
18	0.93 ± 0.18	[1.06 ± 0.20]	0.98 ± 0.21	[1.45 ± 0.30]
20	0.88 ± 0.17	1.03 ± 0.19	0.92 ± 0.20	1.41 ± 0.29
177	0.52 ± 0.15	0.60 ± 0.16	0.52 ± 0.14	0.68 ± 0.16
50% Decimated Mesh Error (mm)				
# of Modes	**Femur-only**	**Joint level (Femur)**	**Tibia-only**	**Joint level (Tibia)**
10	1.18 ± 0.21	1.30 ± 0.25	1.27 ± 0.27	1.66 ± 0.31
12	[1.11 ± 0.21]	1.23 ± 0.22	1.20 ± 0.27	1.62 ± 0.32
16	0.98 ± 0.19	1.12 ± 0.21	1.05 ± 0.22	1.50 ± 0.30
18	0.94 ± 0.19	1.07 ± 0.20	[1.00 ± 0.21]	1.46 ± 0.30
20	0.89 ± 0.18	[1.03 ± 0.19]	0.93 ± 0.19	[1.41 ± 0.28]
177	0.53 ± 0.16	0.61 ± 0.16	0.53 ± 0.15	0.69 ± 0.17

This produced decreased errors as the number of modes increased for the individual SSMs and the Joint-level SSM. When the error is observed at the same number of modes, it is consistently lower for the Femur and Tibia only SSMs when compared to the Joint-level SSM, which was seen in both the full and 50% decimated meshes. Differences observed in overlays between the SSM-predicted and actual geometries were up to 10 mm for the Joint-level SSM and up to 6 mm for the individual SSMs and occurred in critical regions, including the posterior medial femoral condyles and tibial tubercle utilizing the number of modes to reach 95% variance explained for each SSM (Figure 5.6).

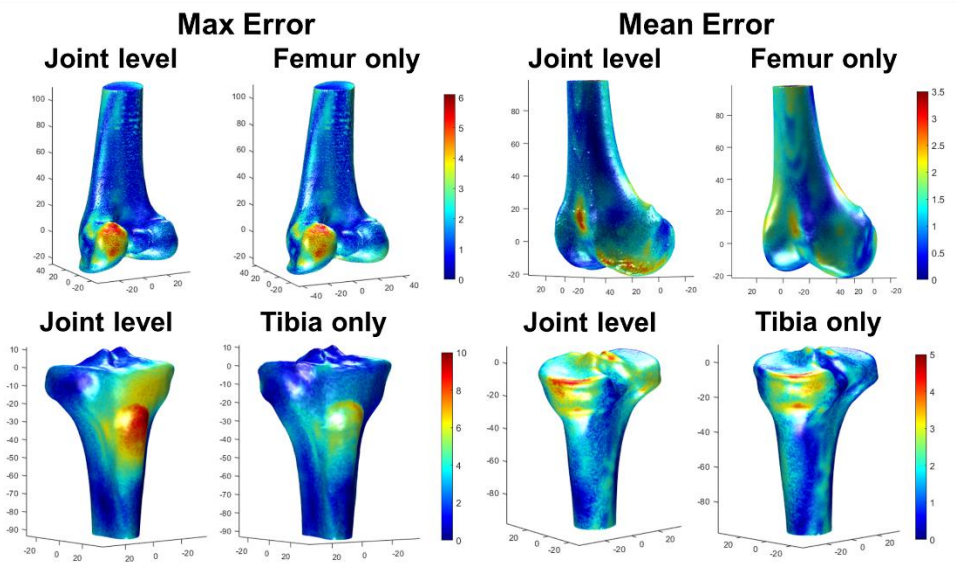

Figure 5.6 Overlay plots from generalization measure that highlight differences for max and mean error subjects using modes based on 95% variation explained.

Lastly, Specificity found the average error for the 1000 random subjects generated, which resulted in smaller errors for the individual bone models when predicting new, random geometries when compared to the Joint-level SSM (Table 5.5). This was observed in both the full mesh and 50% decimated mesh.

Table 5.5 Specificity error results for each of the SSMs for both full mesh and 50% decimated mesh.

Bone	**Full Mesh**	**50% Decimated Mesh**
Femur-only	2.21 ± 1.02	2.32 ± 0.980
Joint-level (Femur)	2.42 ± 1.06	2.49 ± 1.05
Tibia-only	2.14 ± 0.918	2.19 ± 0.927
Joint-level (Tibia)	2.55 ± 1.16	2.53 ± 1.13

5.4 Discussion

SSMs describe the variation in bony anatomy present in the training set; as SSMs move from individual bones to joints with multiple bones, the amount of data in the model increases and this influences the ability to accurately describe the anatomy. From

the compactness measure, it was seen that when comparing the Joint-level SSM to the individual SSMs, more modes were needed to describe a similar amount of variation, specifically to reach 95% variation explained (Table 5.2). Similar behavior was observed in the 50% decimated mesh. These observations was expected considering the large amount of data included in the Joint-level model. It was also determined that when comparing each of the SSMs from the decimated mesh to the full mesh, more modes were needed for the decimated mesh to describe a similar percentage of variation.

The Accuracy measure, describing the ability to represent subjects in the training set, decreased as more modes were included (Figure 5.3). The shape of the observed curves between the individual SSMs and the Joint-level SSMs were similar. However, the individual SSMs showed smaller errors for the same number of modes and more gradual slopes when compared to the Joint-level SSM. For the Femur, using the number of modes corresponding to 95% variation, accuracy was lower for the Joint-level model (0.92 mm) than for the Femur-only model (1.08 mm), but included 8 more modes of variation. For the Tibia, the accuracy was smaller for the Tibia-only SSM (0.91 mm) compared to the Joint-level SSM (1.30 mm) based on a more similar number of modes capturing 95% variation. When a consistent number of modes are included, accuracy for the individual bone SSMs always resulted in less error than the Joint-level SSM. Similarly, the 50% decimated mesh showed higher levels of error in the accuracy measure compared to the full mesh (Table 5.3).

The Generalization evaluation showed the individual bone models were more accurate in describing bone morphology than the Joint-level models (Figure 5.4 and 5.5).

Specifically, errors were smaller for the individual SSMs than for the Joint-level SSM at the corresponding number of modes. When looking at the modes corresponding to 95% variation, the Joint-level prediction of the Femur had an error of 1.06 ± 0.20 mm which was less than the Femur-only SSM error of 1.16 ± 0.21 mm, however, the Joint-level SSM required 8 more modes of variation to achieve a similar error. At 95% variation explained, the Tibia-only SSM had a much smaller error of 1.26 ± 0.28 mm when compared to the Joint-level SSM which resulted in an error of 1.45 ± 0.30 mm as seen in Table 5.4. The same results of the individual SSMs having lower errors than the Joint level SSM were seen for the 50% decimated mesh (Table 5.4). This result was expected as it was hypothesized that the individual SSMs would result in higher accuracy, specifically pertaining to the generalization method. When comparing the full mesh errors to the decimated mesh errors, the full mesh has smaller errors. By comparing the number of modes corresponding to 95% variation, the decimated mesh has lower errors, however, it required more modes of variation. This result was to be expected as the decimation of mesh would result in lower accuracy of the models, specifically in the Generalization measure. The Generalization measure also produced overlay plots at the 95% variation explained, where differences were observed in the posterior femoral condyles, the tibial plateau, and the tibial tubercle (Figure 5.6). In clinical applications, representations of the articular surface and the locations of soft tissue attachment sites must be precise and can influence model predictions of joint mechanics. The accuracy of the predicted bone geometry improved as more modes were included in the generalization evaluation. While utilizing the number of modes corresponding to 95%

variation for each SSM seems reasonable, errors continued to decrease until ~50 modes for the individual SSMs and ~100 modes for the Joint-level SSM.

The Specificity measure showed that the individual bone models had smaller errors when predicting random new geometries than the Joint-level model. Specifically, the Femur-only model was more accurate in creating random new geometry with a mean error of 2.21 ± 1.02 mm than the Joint-level model at 2.42 ± 1.06 mm. Similarly for the Tibia-only model with an error of 2.14 ± 0.918 mm compared to the Joint-level model with an error of 2.55 ± 1.16 mm. The full mesh developed more accurate random new geometries than the 50% decimated mesh did, when comparing the individual bone models and the Joint-level model. Both results were expected, as it was hypothesized that the individual bone SSMs would be more accurate, as well as the full mesh.

The accuracies of these models were comparable to the results seen in the Audenaert et al., 2017 study. Compactness showed similar results, however, Audenaert et al., 2017 required less number of principal components to reach similar levels of variation explained as this study did, which can be attributed to the larger data set that the models were developed with. However, the accuracy levels when compared at the same percentage of explanation had similar errors of 0.59 ± 0.06 mm for both the individual femur and tibia and errors of 0.43 ± 0.07 mm and 0.50 ± 0.07 mm for the femur and tibia respectively for this study (Audenaert et al., 2017). Zhang et al., 2016 used a leave-one-out analysis to determine errors for each bone in a full lower-limb model. Mean errors found for the femur were 4.57 ± 1.75mm and the tibia and fibula at 3.63 ± 0.79 mm (Zhang et al., 2016). These errors were larger than for our joint level femur and tibia for

any number of modes of variation seen for both full and decimated meshes (Figure 5.4 and 5.5). This may be due to differences in sparsity of the nodes of the lower-limb model, as well as, the previous study using full bones versus the proximal tibia and distal femur used in this study. Rao et al., 2013 conducted a leave-one-out analysis on a knee joint that included the distal femur, proximal tibia, and patella. Using the number of principal components that equate to 95% variation explained, the model had a mean error of about 1.6 mm which was larger than the mean error found at the joint-level femur of 0.92 and tibia of 1.30 found in this study (Rao et al., 2013). The models developed in this study resulted in comparable accuracy levels to that of previous studies.

The results of this study show that individual bone SSMs do result in higher accuracies when compared to the Joint-level SSM for these measures. For each of these measures the Joint-level SSM required more modes to achieve similar accuracy to the individual bone models. Still, the tradeoffs with accuracy should be weighed before the determination of the use of an individual bone SSM versus a Joint-level SSM for certain studies. The same can be determined by using decimated meshes, as the full mesh produced more accurate results for these measures. Therefore, the tradeoffs in accuracy need to be determined before the use of a full or decimated mesh setup.

As the training set captures variability in gender and ethnicity, the model's ability to accurately describe unseen subjects gives confidence for use in a range of biomechanics applications. Specifically, anatomic variation, e.g. femur size and width, has been primarily accommodated in implant systems through design and sizing. With robotic surgical techniques providing the ability to precisely control bony cuts and enabling

patient-specific alignment, the development of new implants and surgical plans can thus potentially leverage SSMs and additional modes of variation describing patient anatomy

Chapter Six: Conclusion

6.1 Main Findings

The work presented in Chapter 4 highlights the collection of maximum torque and implantation force during the surgical approach of the revision total hip femoral stem and the micromotion of the femoral stem during static and activities of daily living loading conditions. The reaming torque and implantation force had no correlation to the amount of micromotion seen for the femoral stems. Bone-implant interface micromotion and the kinematics of micromotion of the whole stem to the femur showed increased amounts of micromotion for the gait and stair descent activities versus the static AP and SI loading conditions. In order to accurately determine the amount of micromotion for the initial stability of a femoral stem, the loading conditions of activities of daily living need to be included.

The work presented in Chapter 5 highlights the development of SSMs for individual bones, specifically femur and tibia, and a joint-level model that consists of the femur and tibia modeled as one. This chapter also determined the level of accuracy in which the individual bone models and joint-level models have compared to one another, using measures outlined by Audenaert et al., 2019. Mesh densities of 100% and 50% between the models for these measures were compared. The measures resulted in lower amounts of error for the individual bone when compared to that of the joint-level model,

specifically when looking at the same amount of modes of variation. There was lower amounts of error for the measures in the full mesh models versus the decimated meshes. This chapter suggested that using individual bone models presented higher levels of accuracy than joint-level models, but trade-offs in higher accuracy should be weighed when determining the use of an individual bone versus a joint-level model.

6.2 Future Work

To expand on the research in Chapter 4, the results from this study will be used to develop finite element models of the micromotion setup in the AMTI VIVO. Using the subject-specific models, the amount of micromotion seen in the model will be compared to the results of the in vitro testing conducted. The results of the in vitro test will provide verification for the results of the finite element models and will allow the use of the finite element models to be used in future studies with different femoral stems and different femur models. These models will be used to further analyze implant designs and the micromotion associated with implant decisions.

To expand on the research in Chapter 5, the models will be used to develop random new geometries for future implant designs. The models were found to be comparative to previous models of individual bones and joint-level models for levels of accuracy and thus will provide a large impact in the future for total knee arthroplasty implants to account for the world's population variability. The models will help in the understanding of changes in shape variation between individual bone and joint-level models. This study will be used as an indication for the use of individual bone or joint-

level models in future studies dependent on trade-offs in accuracy for the studies objectives.

References

Andreaus, U., & Colloca, M. (2009). Prediction of micromotion initiation of an implanted femur under physiological loads and constraints using the finite element method. Engineering in Medicine, 223, 589–605. https://doi.org/10.1243/09544119JEIM559

Audenaert, E. A., Pattyn, C., Steenackers, G., de Roeck, J., Vandermeulen, D., & Claes, P. (2019). Statistical Shape Modeling of Skeletal Anatomy for Sex Discrimination: Their Training Size, Sexual Dimorphism, and Asymmetry. Frontiers in Bioengineering and Biotechnology | Www.Frontiersin.Org, 1, 302. https://doi.org/10.3389/fbioe.2019.00302

Baleani, M., Cristofolini, L., & Toni, A. (2000). Initial stability of a new hybrid fixation hip stem: Experimental measurement of implant-bone micromotion under torsional load in comparison with cemented and cementless stems. https://doi.org/10.1002/(sici)1097-4636(20000615)50:4<605::aid-jbm17>3.0.co;2-p

Barr, J. S., White, J. K., Punt, S. E. W., Conrad, E. U., & Ching, R. P. (2015). Effect of simulated early weight bearing on micromotion and pullout strength of uncemented distal femoral stems. Orthopedics, 38(5), e417–e422. https://doi.org/10.3928/01477447-20150504-60

Besl, P. J., & McKay, N. D. (1992). A Method for Registration of 3-D Shapes. IEEE Transactions on Pattern Analysis and Machine Intelligence, 14(2), 239–256. https://doi.org/10.1109/34.121791

Bozic, K. J., Kurtz, S. M., Lau, E., Ong, K., Vail, T. P., & Berry, D. J. (2009). The Epidemiology of Revision Total Hip Arthroplasty in the United States. The Journal of Arthroplasty, 24(2), e19. https://doi.org/10.1016/j.arth.2008.11.033

Bruse, J. L., Zuluaga, M. A., Khushnood, A., Mcleod, K., Ntsinjana, H. N., Hsia, T.-Y., Sermesant, M., Pennec, X., Taylor, A. M., & Schievano, S. (2017). Detecting Clinically Meaningful Shape Clusters in Medical Image Data: Metrics Analysis for Hierarchical Clustering Applied to Healthy and Pathological Aortic Arches. IEEE Transactions On Biomedical Engineering, 64(10). https://doi.org/10.1109/TBME.2017.2655364

Burke, D. W., O'Connor, D. O., Zalenski, E. B., Jasty, M., & Harris, W. H. (1991). Micromotion of cemented and uncemented femoral components. 73(1), 33–37. https://doi.org/10.1302/0301-620X.73B1.1991771

Camine, M.V., Rüdiger, H. A., Pioletti, D. P., & Terrier, A. (2018). Effect of a collar on subsidence and local micromotion of cementless femoral stems: in vitro comparative study based on micro-computerised tomography. International Orthopaedics, 42, 49–57. https://doi.org/10.1007/s00264-017-3524-0

Cerveri, P., Belfatto, A., & Manzotti, A. (2020). Predicting Knee Joint Instability Using a Tibio-Femoral Statistical Shape Model. Frontiers in Bioengineering and Biotechnology, 8. https://doi.org/10.3389/fbioe.2020.00253

Corail® Revision STEM | Surgical Technique | DePuy Synthes. https://www.jnjmedtech.com/en-US/product/corailr-revision-stem

Dai, Y., Giles, Scuderi, R., Penninger, C., Bischoff, J. E., & Rosenberg, A. (2014). Increased shape and size offerings of femoral components improve fit during total knee arthroplasty. Knee Surg Sports Traumatol Arthrosc, 22, 2931–2940. https://doi.org/10.1007/s00167-014-3163-6

Duwelius, P. J., Burkhart, B., Carnahan, C., Branam Bsc, G., Ko, L. M., Wu, Y., Froemke, C., Wang, L., & Grunkemeier, G. (2014). Modular versus Nonmodular Neck Femoral Implants in Primary Total Hip Arthroplasty: Which is Better? Clinical Orthopaedics and Related Research, 472, 1240–1245. https://doi.org/10.1007/s11999-013-3361-4

Feng, S., Zhang, Y., Bao, Y.-H., Yang, Z., Zha, G.-C., & Chen, Y. (2020). comparison of modular and nonmodular tapered fluted titanium stems in femoral revision hip arthroplasty: a minimum 6-year follow-up study. https://doi.org/10.1038/s41598-020-70626-6

Fitzpatrick, C. K., Baldwin, M. A., Laz, P. J., FitzPatrick, D. P., Lerner, A. L., & Rullkoetter, P. J. (2011). Development of a statistical shape model of the patellofemoral joint for investigating relationships between shape and function. Journal of Biomechanics, 44(13), 2446–2452. https://doi.org/10.1016/j.jbiomech.2011.06.025

Gaffney, B. M. M., Hillen, T. J., Nepple, J. J., Clohisy, J. C., & Harris, M. D. (2019). Statistical shape modeling of femur shape variability in female patients with hip dysplasia; Statistical shape modeling of femur shape variability in female patients with hip dysplasia. J Orthop Res, 37, 665–673. https://doi.org/10.1002/jor.24214

Galloway, F., Kahnt, M., Ramm, H., Worsley, P., Zachow, S., Nair, P., & Taylor, M. (2013). A large scale finite element study of a cementless osseointegrated tibial tray. Journal of Biomechanics, 46(11), 1900–1906. https://doi.org/10.1016/j.jbiomech.2013.04.021

Glassou, E. N., Hansen, T. B., Mäkelä, K., Havelin, L. I., Furnes, O., Badawy, M., Kärrholm, J., Garellick, G., Eskelinen, A., & Pedersen, A. B. (2016). Association between hospital procedure volume and risk of revision after total hip arthroplasty: A population-based study within the Nordic Arthroplasty Register Association database. Osteoarthritis and Cartilage, 24(3), 419–426. https://doi.org/10.1016/j.joca.2015.09.014

Goparaju, A., Iyer, K., Bône, A., Hu, N., Henninger, H. B., Anderson, A. E., Durrleman, S., Jacxsens, M., Morris, A., Csecs, I., Marrouche, N., & Elhabian, S. Y. (2022).

Benchmarking off-the-shelf statistical shape modeling tools in clinical applications. Medical Image Analysis, 76, 102271. https://doi.org/10.1016/j.media.2021.102271

Gortchacow, M., Wettstein, M., Pioletti, D. P., & Terrier, A. (2011). A new technique to measure micromotion distribution around a cementless femoral stem. https://doi.org/10.1016/j.jbiomech.2010.09.023

Grood E.S., Suntay W.J., (1983) A joint coordinate system for the clinical description of three-dimensional motions: application to the knee. J Biomech Eng. 1983 May;105(2):136-44. https://doi.org/10.1115/1.3138397.

Gwam, C. U., Mistry, J. B., Mohamed, N. S., Thomas, M., Bigart, K. C., Mont, M. A., & Delanois, R. E. (2017). Current Epidemiology of Revision Total Hip Arthroplasty in the United States: National Inpatient Sample 2009 to 2013. Journal of Arthroplasty, 32(7), 2088–2092. https://doi.org/10.1016/j.arth.2017.02.046

Horn, J. L. (1965). A rationale and test for the number of factors in factor analysis. Psychometrika, 30(2), 179–185. https://doi.org/10.1007/BF02289447

Jasty, M., Bragdon, C. R., Zalenski, E., O'connor, D., Page, A., & Harris, W. H. (1997). Enhanced Stability of Uncemented Canine Femoral Components by Bone Ingrowth Into the Porous Coatings. In The Journal of Arthroplasty (Vol. 12, Issue 1). https://doi.org/10.1016/s0883-5403(97)90055-3

Kwong, L. M., Miller, A. J., & Lubinus, P. (2003). A modular distal fixation option for proximal bone loss in revision total hip arthroplasty: A 2- to 6-year follow-up study. Journal of Arthroplasty, 18(3 SUPPL. 1), 94–97. https://doi.org/10.1054/arth.2003.50083

Lu, H. Y., Shih, K. S., Lin, C. C., Lu, T. W., Li, S. Y., Kuo, H. W., & Hsu, H. C. (2021). Three-Dimensional Subject-Specific Knee Shape Reconstruction with Asynchronous Fluoroscopy Images Using Statistical Shape Modeling. Frontiers in Bioengineering and Biotechnology, 9. https://doi.org/10.3389/fbioe.2021.736420

Mahfouz, M., Fatah, E. E. H. A., Bowers, L. S., & Scuderi, G. (2012). Three-dimensional morphology of the knee reveals ethnic differences. Clinical Orthopaedics and Related Research, 470(1), 172–185. https://doi.org/10.1007/S11999-011-2089-2

Mikkelsen, R. T., Fløjstrup, M., Lund, C., Kjærsgaard-Andersen, P., Skjødt, T., & Varnum, C. (2017). Modular Neck vs Nonmodular Femoral Stems in Total Hip Arthroplasty—Clinical Outcome, Metal Ion Levels, and Radiologic Findings. Journal of Arthroplasty, 32(9), 2774–2778. https://doi.org/10.1016/j.arth.2017.03.072

Mjöberg, B. (2009). Acta Orthopaedica Scandinavica Theories of wear and loosening in hip prostheses: Wear-induced loosening vs loosening-induced wear-a review. https://doi.org/10.3109/17453679408995473

Myronenko, A., & Song, X. (2010). Point set registration: Coherent point drifts. IEEE Transactions on Pattern Analysis and Machine Intelligence, 32(12), 2262–2275. https://doi.org/10.1109/TPAMI.2010.46

Ong, K. L., Day, J. S., Manley, M. T., Kurtz, S. M., & Geesink, R. (2009). Biomechanical Comparison of 2 Proximally Coated Femoral Stems. Effects of Stem Length and Surface Finish. Journal of Arthroplasty, 24(5), 819–824. https://doi.org/10.1016/j.arth.2008.09.012

Pedoia, V., Lansdown, D. A., Zaid, M., McCulloch, C. E., Souza, R., Ma, C. B., & Li, X. (2015). Three-dimensional MRI-based statistical shape model and application to a cohort of knees with acute ACL injury. Osteoarthritis and Cartilage, 23(10), 1695–1703. https://doi.org/10.1016/J.JOCA.2015.05.027

Race, A., Miller, M. A., & Mann, K. A. (2010). Novel methods to study functional loading micromechanics at the stem-cement and cement-bone interface in cemented femoral hip replacements THA Arthroplasty Cement Micromechanics Stem-cement interface Cement-bone interface Micro-motion Cadaver Retrieval. Journal of Biomechanics, 43, 788–791. https://doi.org/10.1016/j.jbiomech.2009.10.021

Rao, C., Fitzpatrick, C. K., Rullkoetter, P. J., Maletsky, L. P., Kim, R. H., & Laz, P. J. (2013). A statistical finite element model of the knee accounting for shape and alignment variability. Medical Engineering and Physics, 35(10), 1450–1456. https://doi.org/10.1016/j.medengphy.2013.03.021

RECLAIM® Modular Revision Hip System | Depuy Synthes. https://www.jnjmedtech.com/en-US/product/reclaim-modular-revision-hip-system

Richards, C. J., Duncan, C. P., Masri, B. A., & Garbuz, D. S. (2009). Femoral Revision Hip Arthroplasty A Comparison of Two Stem Designs. Clinical Orthopaedics and Related Research, 491–496. https://doi.org/10.1007/s11999-009-1145-7

Russell, R. D., Huo, M. H., Rodrigues, D. C., & Kosmopoulos, V. (2016). Stem geometry changes initial femoral fixation stability of a revised press-fit hip prosthesis: A finite element study. Technology and Health Care, 24(6), 865–872. https://doi.org/10.3233/THC-161235

Seim, H., Kainmueller, D., Heller, M., Lamecker, H., Zachow, S., & Hege, H.-C. (2008). Automatic Segmentation of the Pelvic Bones from CT Data Based on a Statistical Shape

Model. G VCBM 2008 - Eurographics Workshop on Visual Computing for Biomedicine, 93-100, https://doi.org/10.2312/VCBM/VCBM08/093-100

Sheth, N. P., Nelson, C. L., Springer, B. D., Fehring, T. K., & Paprosky, W. G. (2013). Acetabular bone loss in revision total hip arthroplasty: Evaluation and management. In Journal of the American Academy of Orthopaedic Surgeons (Vol. 21, Issue 3, pp. 128–139). https://doi.org/10.5435/JAAOS-21-03-128

Singh, J. A., Yu, S., Chen, L., & Cleveland, J. D. (2019). Rates of Total Joint Replacement in the United States: Future Projections to 2020–2040 Using the National Inpatient Sample. The Journal of Rheumatology, 1134–1140. https://doi.org/10.3899/jrheum.170990

Sintini, I., Burton II, W. S., Sade, Sr, P., Chavarria, J. M., & Laz, P. J. (2018). Investigating Gender and Ethnicity Differences in Proximal Humeral Morphology Using a Statistical Shape Model. J Orthop Res, 36, 3043–3052. https://doi.org/10.1002/jor.24070

Siopack J.S., Jergesen H.E.. Total hip arthroplasty. (1995) West J Med;162(3):243-9. PMID: 7725707; PMCID: PMC1022709.

Small, S. R., Hensley, S. E., Cook, P. L., Stevens, R. A., Rogge, R. D., Meding, J. B., & Berend, M. E. (2017). Characterization of Femoral Component Initial Stability and Cortical Strain in a Reduced Stem-Length Design. Journal of Arthroplasty, 32(2), 601–609. https://doi.org/10.1016/j.arth.2016.07.033

Smoger, L. M., Fitzpatrick, C. K., Clary, C. W., Cyr, A. J., Maletsky, L. P., Rullkoetter, P. J., & Laz, P. J. (2015). Statistical Modeling to Characterize Relationships Between Knee Anatomy and Kinematics. J Orthop Res, 33, 1620–1630. https://doi.org/10.1002/jor.22948

Tack, A., Mukhopadhyay, A., Zachow, S. (2018). Knee menisci segmentation using convolutional neural networks: data from the Osteoarthritis Initiative. Osteoarthritis and Cartilage, 26(5), 680–688. https://doi.org/10.1016/j.joca.2018.02.907

Tassani, S., Modenese, L., Dumas, R., Audenaert, E. A., Roeck, D. J., Houcke, V. J., de Roeck, J., Duquesne, K., & van Houcke, J. (2021). Statistical-Shape Prediction of Lower Limb Kinematics During Cycling, Squatting, Lunging, and Stepping-Are Bone Geometry Predictors Helpful? https://doi.org/10.3389/fbioe.2021.696360

Taylor, M., Bryan, R., & Galloway, F. (2013). Accounting for patient variability in finite element analysis of the intact and implanted hip and knee: A review. In International Journal for Numerical Methods in Biomedical Engineering (Vol. 29, Issue 2, pp. 273–292). https://doi.org/10.1002/cnm.2530

Van Dijck, C., Wirix-Speetjens, R., Jonkers, I., & vander Sloten, J. (2018). Statistical shape model-based prediction of tibiofemoral cartilage. Computer Methods in Biomechanics and Biomedical Engineering, 21(9), 568–578. https://doi.org/10.1080/10255842.2018.1495711

Wise, B. L., Liu, F., Kritikos, L., Lynch, J. A., Parimi, N., Zhang, Y., & Lane, N. E. (2016). The association of distal femur and proximal tibia shape with sex: The Osteoarthritis Initiative. Seminars in Arthritis and Rheumatism, 46(1), 20–26. https://doi.org/10.1016/j.semarthrit.2016.02.006